Introduction to Laser Beam and Spectral Measurement 11

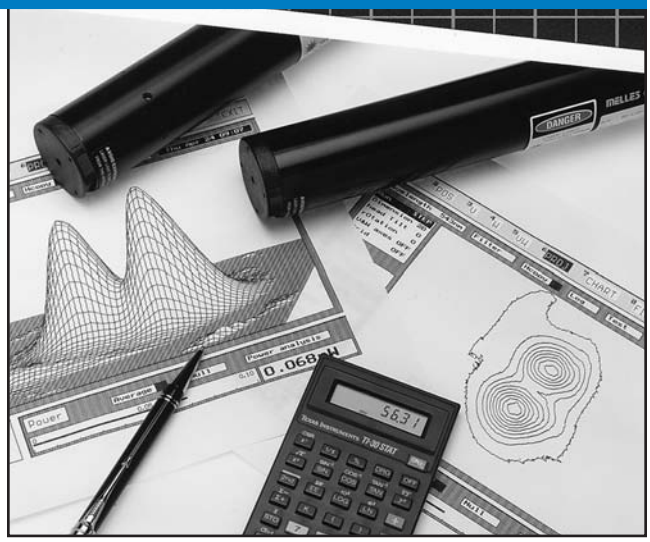

Introduction to Beam Analysis	**11.2**
Fundamentals of Power and Energy Measurement	**11.4**
Fundamentals of Beam Positioning	**11.12**
Fundamentals of Spectral Analysis	**11.15**
Fundamentals of Beam Profiling and Beam Measurement	**11.22**

Introduction to Beam Analysis

It is becoming increasingly important to characterize laser beam parameters fully. The traditional ways of specifying laser beams are necessary, but not sufficient. It used to be that the measurement of wavelength, power, beam width, and mode structure were sufficient for most applications. But there is a significant trend in the photonics industry toward requiring diffraction-limited performance from lasers and optical systems in order to increase the precision and reproducibility with which beams propagate, interact, and can be focused on a target.

CVI Melles Griot provides a complete range of instrumentation to measure not only the traditional parameters, but also difficult-to-measure parameters such as beam profile, propagation factor (M^2), and beam spectral measurements in both wavelength and frequency space. Our instruments take full advantage of state-of-the-art transducers and the full computational and graphic-display capabilities of modern personal computers. Thus this range of instruments provides cost-effective solutions to many laser-beam measurement and characterization needs, both in research and development laboratories and in manufacturing quality-assurance test stations.

CVI Melles Griot instrumentation falls into four broad categories: power and energy measurement, beam-postion measurement, spectral analysis, and beam-intensity profiling.

POWER AND ENERGY MEASUREMENT

One of the most fundamental measurements for a laser is its output power and/or energy. CVI Melles Griot offers complete metering systems (detector head and control/display unit) featuring broadband thermopile and pyroelectric thermal detectors, with flat response from 200 nm to 20 μm, as well as several varieties of photodiode (quantum) power and energy detectors.

Power and Energy Meters

For observing modulated continuous wave (cw) beams, determining pulse shapes, and measuring high-speed noise, we offer a range of high-sensitivity silicon detectors and matching current amplifiers, together with a modular mounting system and a full range of accessories, including integrating spheres.

Photodiodes, Integrating Spheres, and Amplifiers

BEAM-POSITION MEASUREMENT

An unfortunate characteristic of a laser beam is that it changes position as a function of time, age, and atmospheric conditions. In most cases, the movement is only a fraction of a diameter, but in a long-path optical train, even this movement can cause problems. CVI Melles Griot offers

Beam Alignment and Positioning Measurement

four types of systems for measuring beam position and drift: a quadrant detector system for exact centering and alignment, a lateral-effects detector system for measuring larger-scale movement, a dual-detector alignment system that measures both beam position and angular deviation (critical for aligning long-path transfer systems and articulated arms), and a camera-based system for the simultaneous measurement of multiple beams.

SPECTRAL ANALYSIS

A fundamental property of a laser is its wavelength. For many lasers, particularly those operating on narrow atomic transitions, the wavelengths are well defined, at least down to a tenth of a nanometer or less (e.g., the red helium neon lasers output is always 632.8 nm). For broadband lasers, however, this is not the case. A typical dye or titanium-sapphire laser can be continuously tuned over 50 nm or more; the output of a semiconductor diode laser can drift over several nanometers as a function of temperature; some diode-pumped solid-state lasers can be tuned over many nanometers. To measure the fundamental wavelength of a laser, CVI Melles Griot now offers an inexpensive laboratory wavemeter with an accuracy of 0.5 nm. To measure the fine modal structure of the laser beam, we offer two confocal Fabry-Perot optical spectrum analyzers with free spectral ranges (FSRs) of 1.5 GHz and 300 MHz.

In addition to the instruments mentioned above, CVI Melles Griot now offers a variety of Czerny-Turner spectrometers and a spectrophotometer for measuring the spectral content of incoherent sources, as well as a line of spectral-line and illumination sources.

Spectral Analysis

BEAM INTENSITY PROFILERS

For a circular Gaussian beam, knowing the beam-waist diameter and the far-field divergence is sufficient to characterize completely the propagation of that beam through an optical system. Unfortunately, many real laser beams are neither circular nor near-Gaussian. There may be a contribution from higher-order transverse modes; there may be truncation (clipping) or other distortions introduced by lenses, apertures, or other system optics; and the beam itself may be rectangular, elliptical, or completely irregular. Even for a well-behaved near-Gaussian laser beam it is not safe to assume that the divergence and beam-diameter specification indicated on the specification sheet are sufficient to understand the propagation characteristics, since the beam waist is rarely located right at the laser, and, in the near field, divergence is much less than in the far field.

CVI Melles Griot offers the most complete line of beam-intensity profilers in the industry, including pinhole, slit, and knife-edge beam scanners, camera-based profilometers for measuring pulsed and cw sources, and M^2 meters for determining beam propagation characteristics.

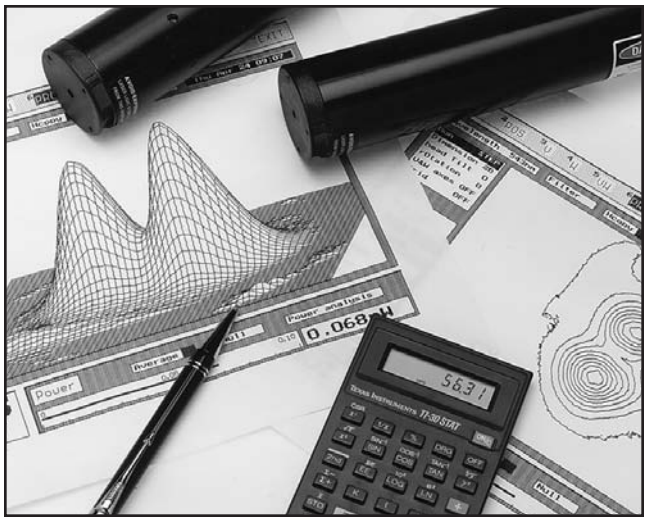

Beam Intensity Profilers and M^2 Measurement

Fundamentals of Power and Energy Measurement

Power and energy detectors can be grouped into two broad categories: thermal detectors and quantum detectors. Thermal detectors simply absorb the incident radiation, increasing the detecting element's temperature until the combined effects of conduction and thermal radiation from the detector are in equilibrium with the energy being absorbed by the detector. The two main types of thermal detectors are thermopiles, used primarily to measure the power of cw laser beams, and pyroelectric detectors, used to measure the energy in a laser pulse. Because thermal detectors measure only the heat generated in the detector, they are extremely broadband, typically with a flat spectral response from 200 nm to 20 μm and beyond.

Quantum detectors operate on a completely different principle. The detector is a semiconductor, and the incident radiation excites electrons from the semiconductor's valence band into the conduction band, generating a current that is proportional to the number of photons in the incident radiation. The gap between the two bands is well defined, and only photons with sufficient energy will be able to move an electron from the valence band to the conduction band. The critical energy λ_c is given by

$$\lambda_c = \frac{hc}{E_g} \qquad (11.1)$$

where h is Planck's constant, c is the speed of light in the semiconductor, and E_g is the energy gap. There are two basic types of quantum detectors: photoconductors, used primarily for measurements in the near infrared (to 5 μm), and photodiodes, used primarily for visible and ultraviolet wavelengths. The sensitivity of quantum detectors is very high, allowing measurements in the picowatt range, and their response time can be much, much faster than that of thermal detectors. On the other hand, their wavelength sensitivity is very nonlinear, their effective wavelength range is much narrower, and they are easily damaged by higher power laser beams.

THERMOPILE DETECTORS

A thermopile detector consists of two sets of thermocouples connected in series (see figure 11.1). One set of thermocouples is attached to an absorbing disc (the detector) and the other set is attached to the case (ambient temperature). As incident radiation is absorbed by the disc, the disc's temperature rises, generating a voltage that is directly proportional to the difference in temperature between the disc and the case. The readout unit then interprets the voltage measurement and presents the information in units of watts (power) or joules (energy).

The detector disc is typically made from graphite or aluminum with a durable, black, absorbing finish. The responsivity of the detector primarily depends upon the thermal mass of the detector disc and the thermocouples mounted to it. The energy is absorbed at the surface and must have time to spread through the detector and bring the disc to a uniform temperature. For larger detectors, used primarily for high-power lasers, this can take several seconds; for smaller detectors, a fraction of a second is typical. To counteract this slow response time, manufacturers often incorporate circuitry in the readout electronics that analyzes the slope of the temperature rise and anticipates

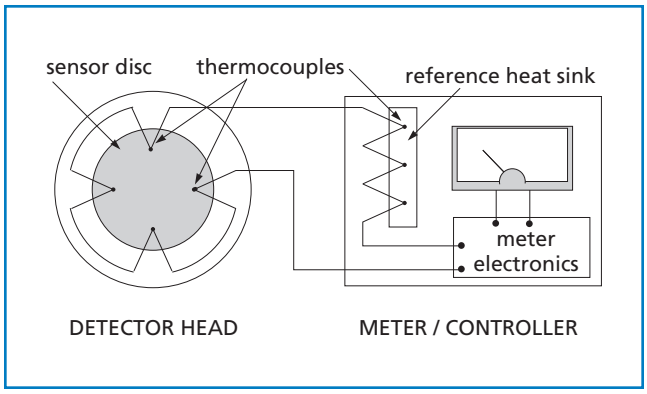

Figure 11.1 **Thermopile Detector**

the equilibrium point. Because of the slow response, thermopile detectors are used primarily for measuring cw output power and average power for pulsed lasers. Peak pulse power and pulse energy measurements are very questionable at rates above a few pulses per second.

PYROELECTRIC DETECTORS

Pyroelectricity and piezoelectricity are closely related. In fact, most piezoelectric crystals also exhibit pyroelectricity. When a pyroelectric crystal is heated or cooled, the stress generated by expansion or contraction generates a voltage across the crystal which is proportional to the rate at which the energy is being absorbed. Either this voltage, or the surface charge on the crystal, can then be measured by a readout unit and converted to watts (peak power) or joules (pulse energy). Unlike a thermopile detector, at thermal equilibrium the voltage across the crystal and the surface charge dissipate, making these detectors unsuitable for cw applications. Detector systems that read the voltage across the crystal are limited to relatively low pulse repetition rates (10's of Hz) because the heat must permeate through the thermal mass of the crystal. Detector systems that measure the surface charge can operate at high pulse rates (>1 kHz) because only the temperature of the crystal at the surface is important; however, at low repetition rates (<10 Hz) the response falls off markedly.

PHOTOCONDUCTORS

Photoconductive detectors are heavily doped semiconductors that have a finite electrical conductivity that increases with temperature. They are used primarily for infrared detection. Typically, the detectors are biased at a fixed voltage, and the current flowing through the detector provides the signal. One problem with photoconductive detectors is that a small change in ambient temperature may significantly increase the dark current (the current flowing through the device when no light is present), swamping the signal. Consequently, either the temperature of the detector must be stabilized or some sort of phase-sensitive detection scheme must be used.

PHOTODIODES

Photodiodes have complex electrical characteristics and can best be understood using the concept of the equivalent circuit—a circuit of individual components (resitors, capacitors, etc.) whose collective (lump-sum) behavior models that of the actual photodiode.

The ideal photodiode can be considered as a current source parallel to a semiconductor diode. The current source corresponds to the current flow caused by the light-generated drift current, while the diode represents the behavior of the junction in the absence of incident light.

An actual photodiode is represented by the equivalent circuit shown in figure 11.2.

In addition to a current source in parallel with a semiconductor diode, a nonconductive layer devoid of carriers (depletion layer) is sandwiched between two conductive layers. This is a classic parallel-plate capacitor, which can support charge separation only in one direction. The effective capacitance, termed the junction capacitance (C_j), is represented in the equivalent circuit by a capacitor in parallel with the other components. The photodiode junction also has finite shunt resistance (R_{sh}). Ancillary parts of the diode (neutral layers, electrical contacts) also give rise to a resistance, usually much smaller than the shunt resistance. This resistance acts between the diode junction and the signal sensing circuit and is therefore termed the series resistance (R_s). The series resistance can usually be assumed to equal zero for modeling and computational purposes.

Photodiode Operation

A photodiode behaves like a photocontrolled current source in parallel with a semiconductor diode and is governed by the standard diode equation:

$$I = I_{\text{photo}} + I_{\text{dk}}\left(e^{qV_0/kT} - 1\right) \qquad (11.2)$$

where

- I is the total device current
- I_{photo} is the photocurrent
- I_{dk} is the dark current
- V_0 is the voltage across the diode junction
- q is the charge of an electron
- k is Boltzmann's constant
- T is the temperature in degrees Kelvin.

The I-V (current-voltage) relationship of this equation is shown in figure 11.3. Two significant features to note from both the curve and the equation are that the photogenerated current (I_{photo}) is additive to the diode current, and the dark current is merely the diode's reverse leakage current. Finally, the detector shunt resistance is the slope of the I-V curve (dV/dI) evaluated at V=0.

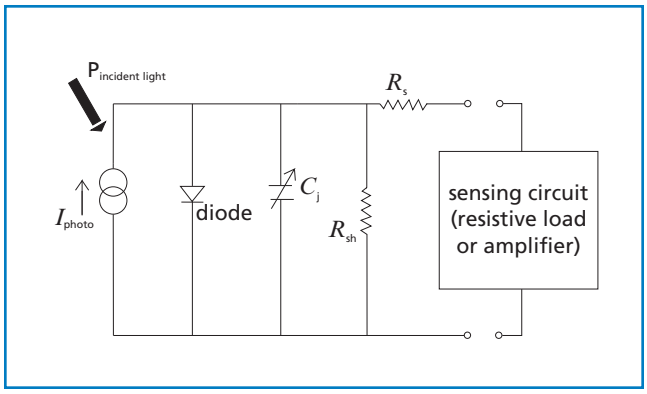

Figure 11.2 **Lumped-sum equivalent-circuit model of a photodiode**

Quantum Efficiency

Photodiodes are quantum devices. Each incoming photon will generate either one or zero units of electron charge which will contribute to the photocurrent. The probability of generating a charge is termed the quantum efficiency (η). Quantum efficiency mainly depends on how efficiently charge carriers are swept across the junction. The overall quantum efficiency of the photodiode is often referred to as external quantum efficiency.

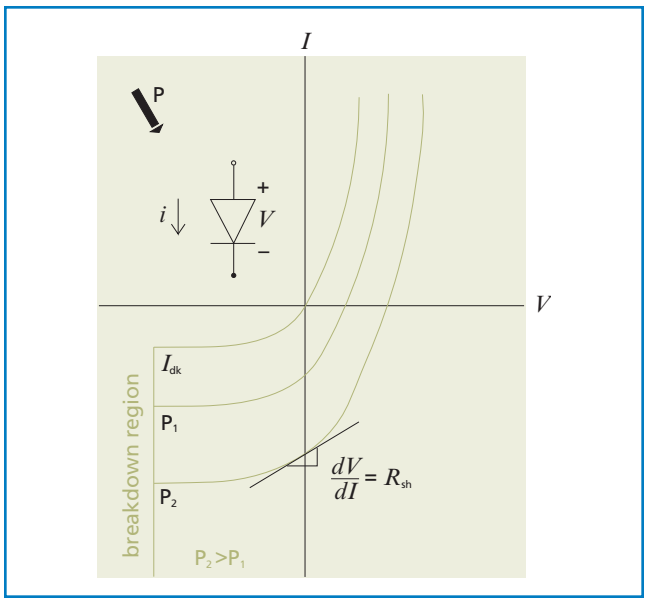

Figure 11.3 **The *I-V* relationship of a photodiode**

Responsivity

Responsivity ($\Re$) quantifies the photoelectric gain of a detector. Photodiode responsivity is the ratio of the photocurrent (across an effective zero resistance) generated for each watt of incident light power, expressed as amps/watt (A/W). Responsivity depends directly on the quantum efficiency. The maximum theoretical achievable responsivity corresponds to detection of every incident photon (unit quantum efficiency). The energy carried by each photon depends on its frequency according to the equation $E = hv$, where v is the photon frequency (inversely proportional to λ, its wavelength) and h is Planck's constant. Therefore, expressing the responsivity in A/W (as opposed to A/photon) gives this parameter an inherent wavelength dependency:

$$\Re = \frac{q\eta\lambda}{hc}$$

or (11.3)

$$\Re = \frac{\eta\lambda}{1.24\times10^{-6}}\ \text{A/W}$$

where

c is the speed of light
q is the charge of an electron
λ is the wavelength in meters of the photons being detected.

Responsivity has an additional wavelength dependence arising from the variation of quantum efficiency with wavelength. At wavelengths where silicon does not absorb strongly, photons may penetrate more deeply into the device (or pass through it), leading to minority carrier generation too remote from the junction to be detected (i.e., lower quantum efficiency). The typical shape of the silicon photodiode responsivity spectral curve is determined by the absorption spectrum of silicon (see figure 11.4). Photodiode responsivity is usually specified at a single wavelength unless a complete wavelength calibration is performed.

As an example, a silicon photodiode normally will have a high quantum efficiency for light at 800 nm. Assuming a typical η of 0.8 at this wavelength, this leads to a responsivity of 0.52 A/W. At 400 nm a typical η would be only 0.15, which leads to a responsivity of 0.1 A/W.

Responsivity alone is a weak figure of merit because it specifies only the gain of a photodiode, not its associated noise. Signal-to-noise ratio represents the ultimate figure of merit, as discussed later.

Linearity of Response

In many applications it is necessary for the responsivity to remain constant over a wide range of incident light power. Most P-N silicon photodiodes are linear (better than 1%) over seven or eight orders of magnitude. However, when the number of incident photons becomes comparable to the number of electron-hole locations in the active region, the device saturates, resulting in a loss of linearity.

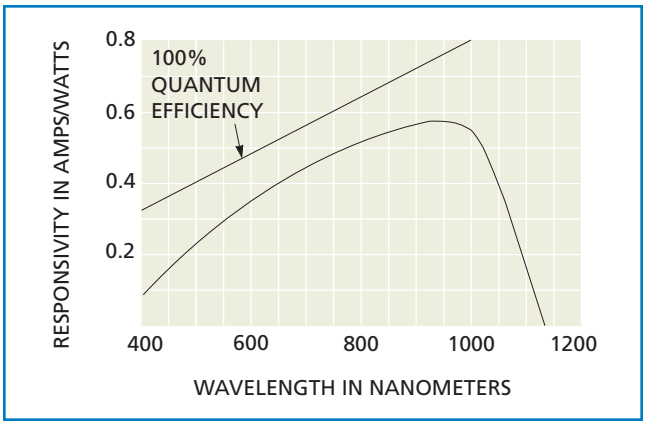

Figure 11.4 **Typical responsivity of a CVI Melles Griot silicon photodiode**

In the case of the CVI Melles Griot silicon photodiodes, the photocurrent will have a linear relationship to the incident intensity, providing the current density is less than 5×10^{-5} A/mm^2. The maximum allowable radiant intensity is therefore given by:

$$\text{Intensity} < \frac{5\times10^{-5}}{\Re}\ \text{W/mm}^2$$

where $\Re$ is the responsivity at the detection wavelength in A/W.

It is important to understand this limitation when using a photodiode to detect laser radiation. The raw output beam from a 1-mW HeNe laser has more than twice the intensity (W/mm^2) necessary to saturate a typical silicon photodiode.

System linearity is also affected by the sensing circuit. Incident light on the photodiode's active area produces a photocurrent which is usually measured by the amount of voltage dropped across an external resistance of known size. As the resultant voltage in the sensing circuit increases, the photodiode becomes forward biased, leading to nonlinear response.

Junction Capacitance

When designing a sensing circuit to maximize the speed or linearity of response, one must know two important electrical characteristics of a photodiode: the junction capacitance (C_j) and the shunt resistance (R_{sh}). Without these, the RC time constant of the complete operating circuit cannot be calculated.

The parallel-plate capacitance across the depletion region gives rise to a junction capacitance which increases with the area of the junction. Since increasing capacitance in a circuit slows its speed of response, photodiodes with smaller active areas are inherently capable of faster response than those with larger active areas. The junction capacitance is a function of the thickness of the depletion layer, which varies with applied bias

(see figure 11.5). Therefore, it is common to specify the junction capacitance at zero external bias. This topic is covered in the discussion on reverse bias operation of photodiodes.

Detector Angular Response

The photocurrent generated from a photodiode is essentially independent of angle of incidence of the incoming radiation when the angle of incidence is less than 30 degrees. Typically, a variation in photocurrent of 1 to 2 percent can be expected, provided the detector's active area is underfilled, i.e., the incoming radiation does not completely cover the device's entire active area. (This condition assumes the photodiode's absorption layer thickness approximately equals the depletion layer thickness in the photodiode junction.)

In circumstances where the photodiode is immersed in a collimated beam of incident light, the device's responsivity will fall off with the cosine of the angle of incidence as follows:

$$\Re_\theta = \Re \cos\theta \qquad (11.4)$$

where $\Re$ is the photodiode responsivity at normal incidence.

Photodiode Speed of Response

Inherent limitations of photodiode response are due to structure and specific junction design, the presence of an externally applied bias, and the wavelength of incoming radiation. The inherent time constant of a photodiode causes a delay in generated photo current (τ). For CVI Melles Griot silicon photodiodes, this time constant is typically 7 to 15 nsec. The photodiode speed of response for various load conditions is discussed in the section on sensing circuits for photodiodes.

Dark Current

The P-N junction of a photodiode does not present an infinite resistance to reverse current flow. Consequently, when a reverse bias is applied to a photodiode, a small current (I_{dk}) flows even in the absence of incident light, as shown in the I-V curve. This dark current increases slowly with increasing reverse bias. Dark current approximately doubles every 8°C.

A large dark current is undesirable since it may represent a significant background above which the actual photocurrent is measured. Furthermore, shot noise associated with the dark current may be significant.

Breakdown Region

There is a maximum reverse bias voltage that can be applied to a photodiode, called the reverse breakdown voltage. At this point, the device is no longer useful as a photodetector and can sustain permanent damage. Care should be taken to limit the current through the diode in the reverse bias region so that the resultant power dissipated does not exceed 200 mW.

Noise-Equivalent Power and Signal-to-Noise Ratio

Noise-equivalent power (NEP) is the incident light level impinging on a photodiode, which produces a photocurrent equal to the noise level. It is usually regarded as the most significant figure of merit for a photodetector. The NEP is a function of the photodiode's responsivity, the noise of the photodiode and the associated sensing circuit, and the frequency bandwidth over which the noise is measured. In systems applications, the signal-to-noise Ratio (SNR) may be computed by taking the ratio of the incident optical power to the photodiode NEP.

In general terms, NEP is defined as follows:

$$\lambda_c = \frac{hc}{E_g} \qquad (11.5)$$

where $\Re$ is in A/W.

The rms noise current (i_{rms}) is the total integrated noise over the frequencies of interest (f_1 to f_2), defined as follows:

$$i_{rms} = \sqrt{\left[i_1^2(f) + i_2^2(f_N) + \ldots i^2(f)\right] df} \qquad (11.6)$$

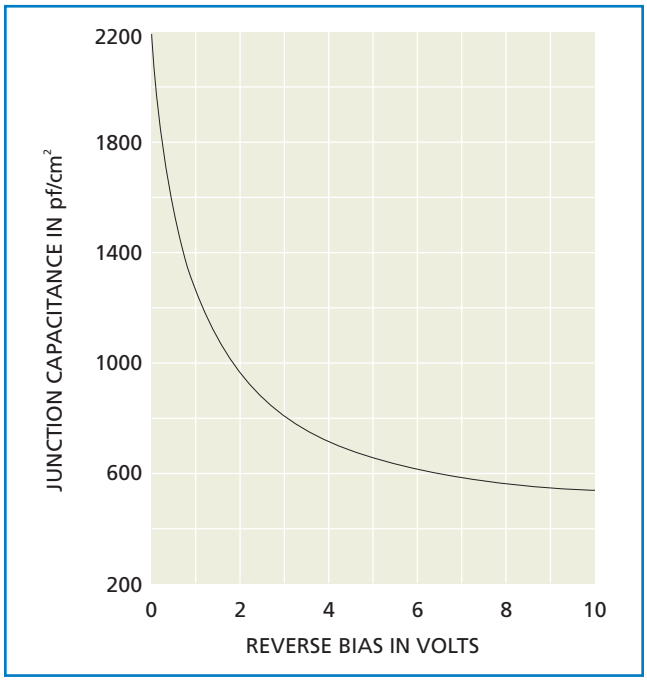

Figure 11.5 **Typical relationship of a silicon photodiode's junction capacitance and applied bias**

If the bandwidth over which the noise is integrated is 1 Hz at frequency f, this is referred to as the noise spectral density at frequency f, with units of W/Hz$^{1/2}$. Since the rms noise is highly dependent upon system application, it is common for noise sources to be specified in terms of noise spectral density at a specific frequency. Since the noise will vary with wavelength, frequency, and temperature, all pertinent parameters must be specified when discussing NEP. The nomenclature NEP (λ, f, T) delineates the specification at wavelength λ, frequency f, and temperature T.

Noise Sources

The lower detection limit for any photodetector is ultimately determined by the device's noise characteristics. There are three main contributions to photodiode noise: Johnson noise, shot noise, and 1/f noise (see figure 11.6.)

Johnson Noise

The statistical fluctuation in the thermal electron-hole pair generation is called thermal noise or Johnson noise (I_{Rsh}). Johnson noise is broadband "white" noise and is expressed as noise per unit bandwidth. The expression for Johnson noise of the photodiode shunt resistance is as follows:

$$I_{R_{sh}} = \sqrt{\frac{4kT}{R_{sh}}}\ \mathrm{A}/\sqrt{\mathrm{Hz}} \qquad (11.7)$$

where

k is Boltzmann's constant
T is the absolute temperature in degrees Kelvin
R_{sh} is the shunt resistance in ohms.

As seen from the above formula, Johnson noise increases in proportion to the square root of the temperature.

Shot Noise

Shot noise (I_{sh}) is the statistical noise associated with the photocurrent and dark current (if present). Since shot noise is also broadband, it is expressed as noise per unit bandwidth:

$$I = \sqrt{2q\left(I_{\mathrm{photo}} + I_{\mathrm{dk}}\right)}\ \mathrm{A}/\sqrt{\mathrm{Hz}} \qquad (11.8)$$

where

q is the charge carried by an electron
I_{photo} is the photocurrent
I_{dk} is the dark current.

1/f Noise

The mechanism for 1/f noise is not particularly well understood. Often the characteristics are empirically determined for individual families of photodetectors. The 1/f noise is governed by the following characteristics:

$$I_{1/f}(s) = I_0\left(\frac{1}{s}\right)^{\alpha}\ \mathrm{A}/\sqrt{\mathrm{Hz}} \qquad (11.9)$$

where

I_0 is typically an inverse function of the active area
α is an empirically derived constant that will vary from 0.25 to 1.0 depending upon the specific construction of the detector
s is the Laplace operator and $= j\omega$.

1/f noise is of concern at frequencies below 100 Hz. For higher frequency applications, photodiode performance is limited by other noise sources. 1/f noise is zero at zero bias.

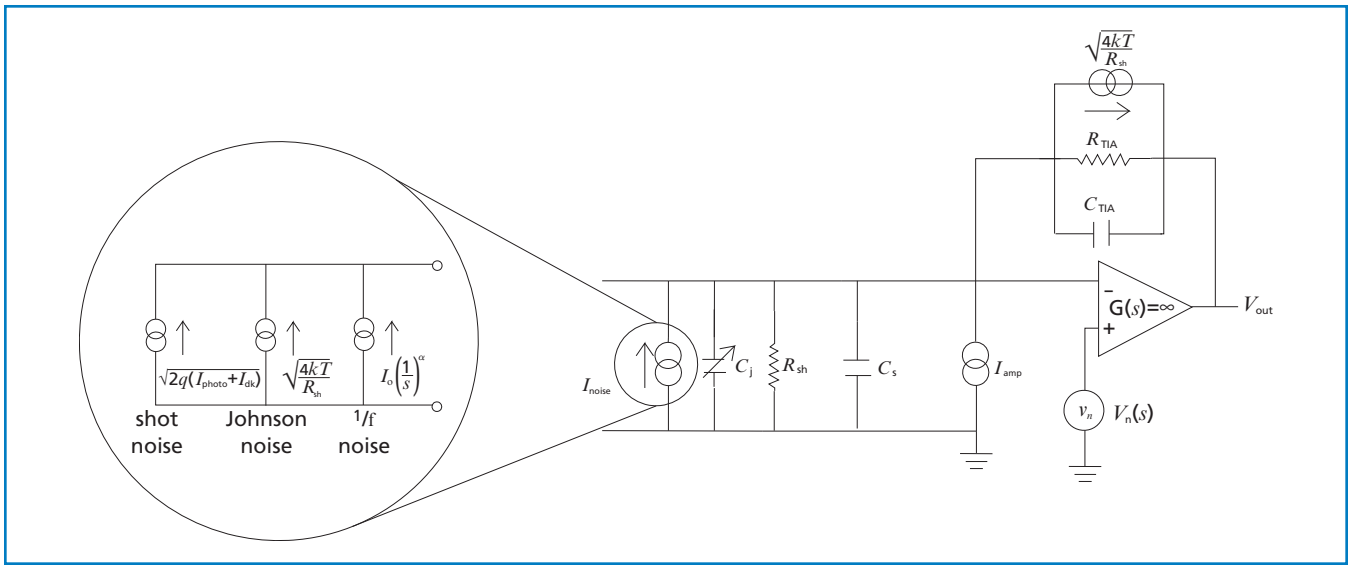

Figure 11.6 **System noise model of a detector and transimpedance-amplifier setup**

Temperature Effects

Like all semiconductor devices, photodiodes are temperature sensitive. The relative population inversion of electrons and holes in the P- and N-layers of the photodiode is directly influenced by temperature, which changes the conductivity and shifts the absorption spectrum. The major photodiode parameters that are sensitive to temperature are shunt resistance, dark current, and, to a lesser extent, responsivity. Typically, the dark current of a silicon photodiode approximately doubles for each 8°C increase or decrease in the device temperature. The shunt resistance approximately doubles for each 6°C change:

These formulas can be used to calculate the shunt resistance and dark current for any temperature from the specified values, which are usually specified at 25°C.

$$I_{dk}(T_2) = I_{dk}(T_1)2^{\frac{(T_1-T_2)}{8}} \qquad (11.10)$$

$$R_{sh}(T_2) = R_{sh}(T_1)2^{\frac{(T_1-T_2)}{6}} \qquad (11.11)$$

Increasing the temperature of a semiconductor shifts its absorption spectrum to longer wavelengths by reducing the effective band gap. Fortunately, the absorption spectrum of silicon is quite broad. Consequently, the small temperature-induced shifts in the absorption spectrum affect the responsivity significantly only at the edges of the spectral responsivity curve, as shown in figure 11.7.

INTEGRATING SPHERES

In many applications of photodetectors, it is necessary to measure the absolute or relative intensity of a wide-angle beam (divergent source) or of an inhomogeneous beam much larger than the active area of a photodetector. Integrating spheres have been used for many years to scramble or average light by multiple diffuse reflections in order to obtain meaningful intensity measurements of these types of sources.

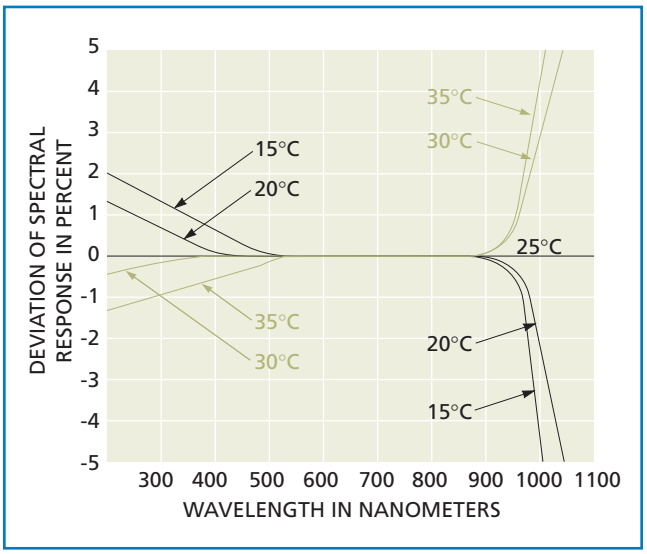

Figure 11.7 **Temperature dependence of silicon photodiode responsivity**

An integrating sphere is a hollow sphere (often aluminum) whose entire inner surface is uniformly coated with a layer of matter which has a highly diffuse reflectance. When light from a source enters an integrating sphere, it loses all memory of direction and polarization. At the exit port, the light intensity is uniform and diffuse. Although other methods have been developed to deal with the problems of averaging the intensity from an inhomogeneous source or of a wide-angle beam, an integrating sphere is the best solution in many applications. In fact, the only real differences between the integrating spheres of today and the spheres of many years ago are the improved quality and stability of the diffuse reflectance coating.

Lambertian Source — Radiance and Irradiance

The two keys to the operation of an integrating sphere are the coating on the inside of the sphere and the spherical shape itself. The coated interior surface is designed to have a highly diffuse reflectance. When a hypothetically perfect diffuse reflector is illuminate with uniform intensity, it behaves like a perfectly diffuse source—a *Lambertian* source (i.e., each unit area reflects light into all available solid angles with equal efficiency).

The complete definition of a Lambertian source is a light source whose radiance is independent of viewing angle. The most well-known Lambertian source is the sun. Radiance is defined as the energy flux per unit projected area per unit solid angle leaving a source or, in general, any reference surface.

Radiance, L, can be expressed as

$$L = \frac{dI}{d\Omega dA\cos\theta} \qquad (11.12)$$

where

dI is the intensity
$d\Omega$ is the solid angle
dA is the unit area of the source
$\cos\theta$ is the viewing or inclination angle.
$dA\cos\theta$ is the projected surface area.

To understand the operation of the integrating sphere, consider the light reflected from a uniformly illuminated small area of the interior surface. This unit area is so small that it can almost be considered a point source. This virtual point source radiates equal intensity in all possible directions. The rest of the sphere can be thought of as a target over which the light from this source will be distributed. Two counterbalancing factors ensure that this light will be distributed with equal intensity over the entire target surface. The important intensity parameter for a target surface is the incident energy (flux) per unit area. This is termed the *irradiance* of the target surface.

The inverse square law shows that the light flux per unit area will be a minimum at the most distant point on the sphere. However, the irradiance of a unit area of the target surface depends on its angle of inclination to the source. A large angle of incidence causes the incident flux to be spread over a large target area (cosine projection). A small angle of incidence presents the smallest area to any incident light. The same cosine projection argument applies to the projected area of the source.

The two effects exactly cancel each other so that the light intensity is uniform over the entire area of the sphere. This can be proven by simple geometry, as shown in figure 11.8.

Consider a small unit area of irradiating surface (dA_s), and a small unit area of target surface (dA_t). The intensity of light (irradiance) α on the target due to the source dA_s is given by:

$$\alpha = L\left(\frac{\cos^2\theta}{d^2}\right)dA_s \qquad (11.13)$$

where L is the source radiance and θ is the angle of incidence on dA_t. The d^2 term is from the inverse square law, and the $\cos^2\theta$ term relates to the effective (cosine projected) areas of the source and target.

In a real application, when an extended area of the surface is illuminated with nonuniform intensity, the directly illuminated spot on the sphere can be considered as a large number of minute Lambertian sources. In principle, therefore, the total flux of the beam entering the sphere is spread (averaged) over the entire surface following only a single reflection.

In order to deliver reliable integration and low throughput loss, the coating of the integrating sphere must be a very efficient diffuse reflector. Coatings used on integrating spheres provide reflection efficiencies between 95 and 99 percent. The reflectance must be high in order to minimize absorption loss caused by multiple reflections, but it must not reflect light in a specular sense (incidence angle=reflectance angle). Any specular component to the reflections off the surface will only help preserve some memory of original angular and spatial distribution of the light source. In many applications, it is also necessary that the properties of the coating be fairly insensitive to wavelength.

Light is not completely averaged or integrated on the first reflection. To prevent erroneous readings that are dependent on input angle, the detector or output port is often shielded with a baffle plate. This small metal plate, also coated with the same diffuse reflectance material, is positioned to preclude any light from the entrance port from reaching the detector after only a single reflection.

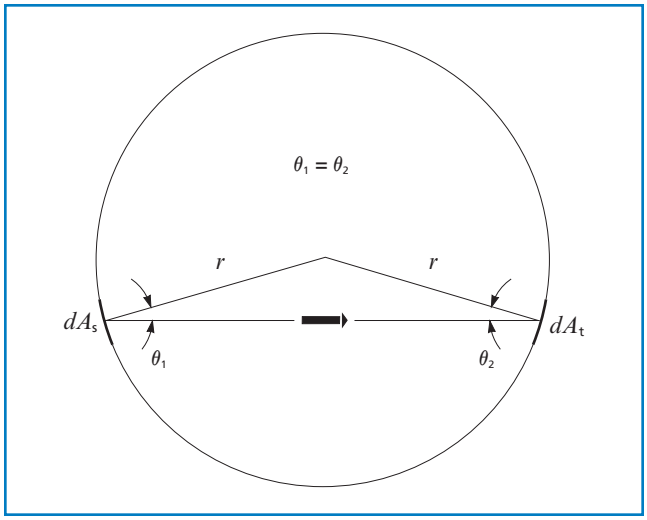

Figure 11.8 **Integrating sphere geometry factors**

Performance Characteristics

Two meaningful figures of merit for integrating spheres are *throughput* and *stability*. Throughput is defined as the ratio of the flux exiting the sphere to the flux entering the sphere. It is determined by the size of the ports (input and exit) relative to the sphere area and by the reflectivity.

$$\text{Throughput} = \frac{A_e R}{\left[1 - R\left(1 - A_p\right)\right]} \qquad (11.14)$$

where

A_e is the area of the exit port divided by total sphere area
R is the reflectance of the coating
A_p is the total area of all ports divided by total sphere area.

Figure 11.9 shows the reflectance of a typical integrating sphere coating.

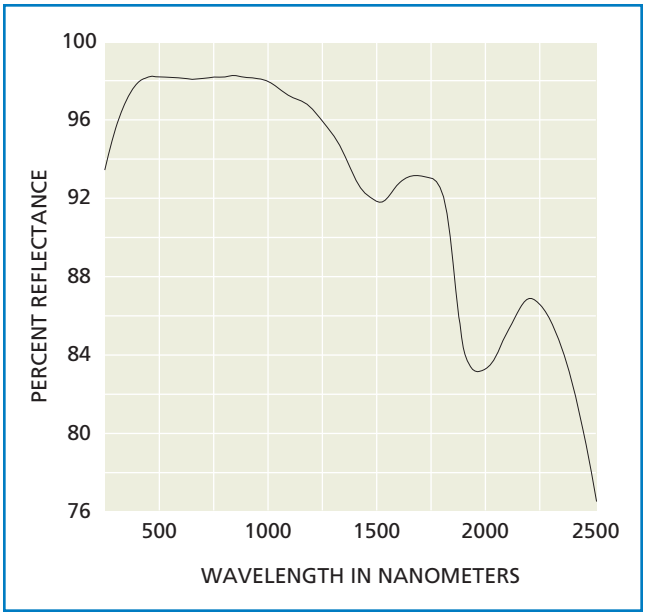

Figure 11.9 **Typical reflectance of the integrating sphere coating**

Throughput is very dependent on the reflectance of the sphere surface in a nonlinear manner (see figure 11.10).

Stability is the reciprocal of the change in throughput with respect to the change in reflectivity of the coating. This is an important parameter since the reflectivity of the coating may degrade slightly in certain operating environments over a long period of time, and the reflectivity may be degraded nonuniformly over the sphere surface. A small change in the reflectivity of a low-stability sphere will result in a large change in throughput. Therefore, a low-stability sphere is less likely to give an accurate, reproducible reading than a high-stability sphere.

Stability is related to throughput. A high-throughput sphere is inherently less stable than a lower-throughput sphere because of the nonlinear dependence of throughput on reflectivity. Stable spheres have reflectivity values of 90 percent or less, whereas the low-stability (high-throughput) spheres typically have reflectivities of 97 percent or greater. As an example, a typical low-throughput sphere with a 90 percent reflectivity coating will have an inherent stability factor of 0.5, whereas an identical high-throughput sphere with a 99 percent reflectivity coating will have a stability factor of 0.05.

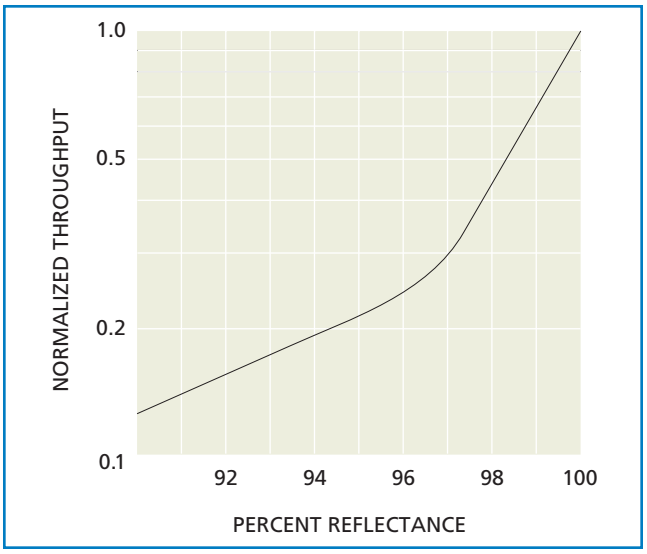

Figure 11.10 **Normalized throughput variation with reflectance for an integrating sphere**

Diverse Applications

Integrating spheres are versatile devices which are used in a wide range of applications. This versatility is best illustrated by the examples outlined below.

1. Diode Laser and Fiber-Optic Power Measurements. Integrating spheres are ideal for collecting and measuring the highly divergent radiation typical of diode lasers and fiber optics.

2. Intensity Measurements of Extended Sources. Tungsten filaments, plasma discharges, and other extended sources can be difficult to collimate or efficiently image onto a photodiode of limited area. The large entrance port of the CVI Melles Griot 13 ISP 005 integrating sphere facilitates coupling in light from extended sources and reduces the need for a complicated optical system.

3. Absolute Radiometry in Anamorphic Laser Systems. An integrating sphere and a large-area detector can accurately measure radiation that is too large to focus onto a detector, or light that is collimated in one plane but defocused in the other. A typical application is measuring the output from laser line projectors.

4. Measurement of Inhomogeneous Beams. The integrating sphere effectively scrambles the input radiation so that any beam inhomogeneity and detector nonuniformities do not affect the accuracy of the measurement.

5. Creation of a Uniform Intensity Profile. An integrating sphere can be used as a transmissive component to homogenize the spatial intensity profile of a beam from an inhomogeneous source. Uniform illumination is required in applications such as calibrating CCD, CMOS, and photodiode arrays.

Fundamentals of Beam Positioning

Position-sensitive detectors (PSDs), which detect and record the positions of incident light beams, find application in the analysis of light sources and industrial alignment of machinery and targets (when used in conjunction with a laser).

Three types of detectors are used for sensing the position of the centroid of a beam in the x-y plane orthogonal to the optic axis: the quadrant detector, the dual-axis lateral-effect detector, and camera-based detectors (CCD or CMOS). In the case of the quadrant and lateral-effect detectors, four electrodes are attached to a large-area silicon detector, and the four currents generated by photoabsorption are processed with the appropriate algorithm to give the x and y positions. In the camera-based systems, the beam position is determined by measuring the intensity of light impinging on each pixel. The quadrant and lateral-effect detectors are discussed in more detail in the next paragraphs. Camera-based detectors are available from CVI Melles Griot in 1/2-inch (CCD) or 1/3-inch (CMOS) formats.

QUADRANT DETECTORS

The quadrant detector is a uniform disk of silicon with two 10-μ-wide gaps across the surface. Thus, there are four independent and equal photodetectors on the sensing surface. The center of the detector is known very accurately since it is the mechanical intersection of the two gap lines and does not change with time or temperature. A symmetrical laser or other optical beam centered on the detector will generate equal photo currents from each of the four sectors. If the beam moves from the center of the detector, the currents from the four sectors will change, and the processing algorithm will give the x and y displacements relative to the center.

Figure 11.11 illustrates the geometry of the quadrant and lateral-effect detectors.

In the quandrant detector, the four sectors are represented by letters A, B, C, and D.

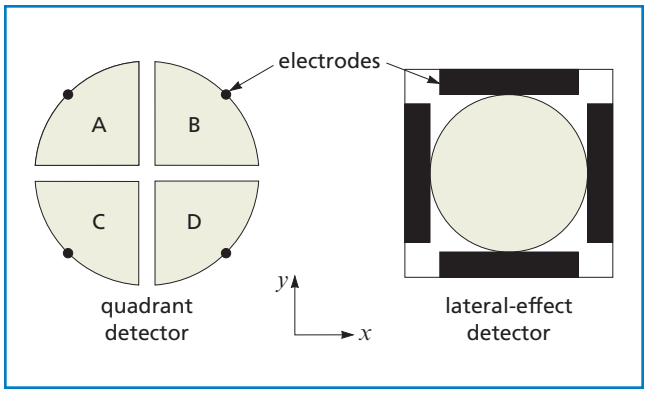

Figure 11.11 **Physical configuration of the quadrant and lateral-effect detectors**

The equations used to describe the x and y displacements of the beam are the following:

$$x = \frac{(b+d)-(a+c)}{a+b+c+d} \qquad y = \frac{(a+b)-(c+d)}{a+b+c+d} \tag{11.15}$$

where a, b, c, and d are the currents generated by each of the four sectors. There are two significant restrictions on the motion of beams used with quadrant detectors. First, to give x-y data, the beam must always overlap a portion of all four sectors. Second, there is only meaningful absolute position information for small displacements of the beam.

The limits of the 8-mm-clear-aperture CVI Melles Griot quadrant detectors are illustrated in figure 11.12.

As shown, if a beam is 2 mm in diameter, its center can move a maximum of 1 mm in any direction before it no longer overlaps all the quadrants. Therefore, the center of the beam must remain within a 2-mm-diameter circle, centered on the detector. The motion of beams larger than 4 mm in diameter is restricted by the clear aperture of the detector rather than the quadrant overlap requirement. Consequently, the center of a 6-mm-diameter beam can only move 1 mm in any direction without moving outside the clear aperture and losing part of the signal.

Because most laser beams are circular with Gaussian intensity distributions, the photocurrents become nonlinear for displacements of more than about 10 percent of the beam radius. Therefore, absolute x and y coordinates become unreliable for beam displacements that are greater than the "measuring limit" shown in figure 11.12.

Because of these two restrictions, the quadrant detector is most useful in systems where a beam must be aligned or centered to an optical axis. It is especially useful where it is necessary to monitor small displacements over long periods with high stability. In feedback systems, displacement information from the quadrant cell is used to realign (null) a laser beam.

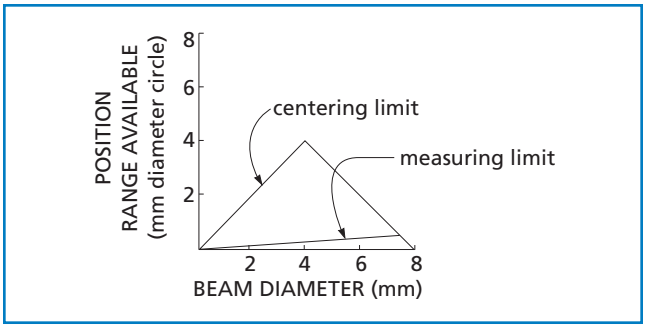

Figure 11.12 **Beam size vs position range for our quadrant detector**

DUAL-AXIS LATERAL-EFFECT DETECTOR

The dual-axis lateral-effect detector uses a doped disk of silicon with four electrodes connected around its perimeter. Opposite pairs of electrodes yield photocurrents that can be processed to give unique values of x and y displacement.

Traditionally, the algorithm has been performed with fixed electronic circuitry, and positions have been accurate to a few percent. The CVI Melles Griot lateral-effect detector employs a software-controlled algorithm and stored calibration corrections to linearize the detector response across the entire sensing area. Unlike the quadrant detector, the dual-axis lateral-effect detector can be used to measure accurately the absolute position of a beam over its entire surface.

Figure 11.13 illustrates the position-measurement limit for the 8-mm-diameter CVI Melles Griot dual-axis lateral-effect detector system. In contrast to a quadrant detector, very small beams can move over the entire 8-mm-diameter surface of the lateral-effect detector. However, because a beam must remain entirely within the area of the detecting surface, larger beams have a limited range of travel. For example, the centroid of a 4-mm-diameter beam must remain within a 4-mm-diameter circle centered on the detector.

Because the lateral-effect detector can accurately measure beam position across its entire surface area, it is frequently used to measure large relative motion of beams and machinery.

APPLICATIONS OF POSITION-SENSING DETECTORS

Position-sensitive detectors (PSDs) are used in numerous laboratory and industrial applications to measure displacements of one form or another. Figures 11.14 through 11.18 illustrate typical setup configurations. In the manufacturing process they characterize lasers and align optical systems. When used in conjunction with lasers they can be used for industrial alignment, calibration, and analysis of machinery.

The following PSD applications are intended to provide examples; they are not meant to be definitive. It would be impossible to list all the uses of these devices. Contact an applications engineer at your nearest CVI Melles Griot office for assistance in evaluating your application's requirement for PSDs.

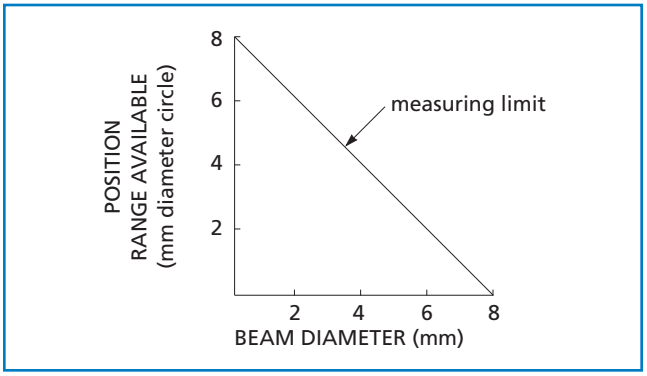

Figure 11.13 **Beam size vs position range for an 8-mm-diameter dual-axis lateral-effect detector**

Laser Testing

Laser manufacturers frequently use PSDs to characterize their collimated lasers. Using a calibrated beamsplitter and two PSDs in the arrangement shown in figure 11.14, one can test the absolute power and power fluctuation of the laser as well as the beam drift, centration, and alignment of the beam to the outer housing or tube. The CVI Melles Griot position-sensing detector systems are particularly well-suited to this application since they provide a graphic target display for tracking beam movement, and a strip chart display to monitor beam characteristics over time.

Measuring Errors in Slideways

In conjunction with a laser, a lateral-effect detector can measure tolerances in slideways with high precision (see figure 11.15). The detector is rigidly mounted perpendicular to a traveling carriage. A laser is aligned to the detector to define a straight optical path. As the carriage moves along the way, the detector measures beam position changes in two axes perpendicular to the direction of motion. Changes in beam position indicate deformities in the rails, play in the bearings, or both.

Where long travel is expected, and/or strain induced by the detector head cable is not tolerable, the PSD can be replaced by a corner-cube retroreflector. The detector is mounted parallel to the laser, and light is reflected back into the PSD. Beam position readings will be twice the actual carriage movement. Similar PSD-based metrology can measure characteristics such as surface flatness.

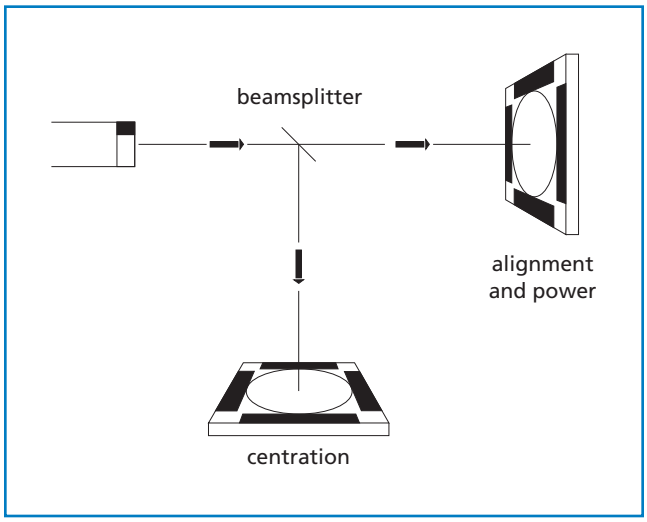

Figure 11.14 **Monitoring laser power, centration, and alignment**

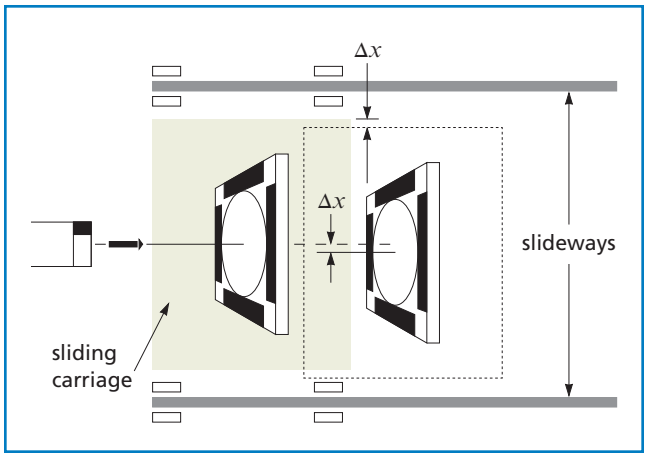

Figure 11.15 **Measuring errors in slideways**

Measuring Roller Parallelism

In industries where materials such as textiles and paper are roll-fed, roller parallelism can be crucial. A laser and a PSD are often used to align and measure this parallelism (see figure 11.16). A laser is mounted onto a V-block with two bubble levels. The V-block is placed on the first roller and leveled in two axes. A PSD with an attached focusing lens is aligned (nulled) to the laser beam, and the V-block is transferred to the second roller, which is then adjusted so that the laser beam is nulled to the PSD. After alignment, the rollers are parallel. The difference between the beam position reading from the first roller and that from the second roller can be divided by the focal length of the lens to yield the angular accuracy of parallelism in radians.

Controlling Optical Beam Alignment

In certain applications it is necessary to align a laser beam to a target and maintain the alignment with extreme precision over long periods of time (see figure 11.17). An active feedback loop maintains alignment by nulling

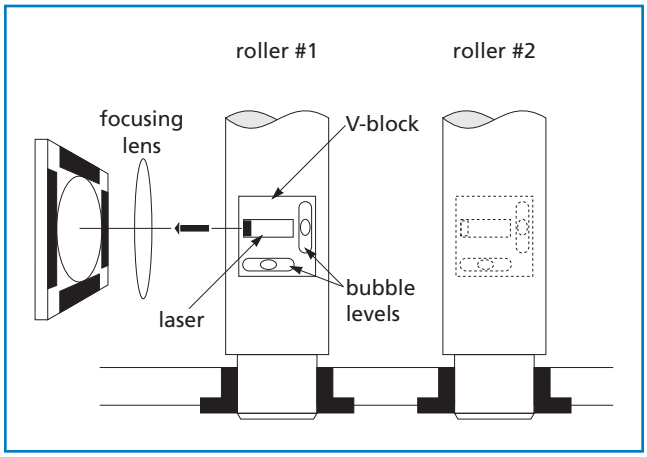

Figure 11.16 **Measuring roller parallelism**

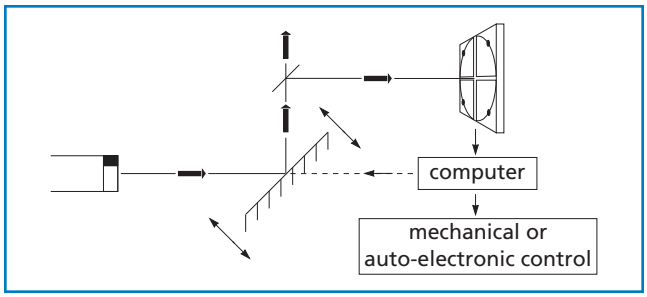

Figure 11.17 **Controlling optical beam alignment**

the beam to the center of the target. Quadrant detectors are often used as the target in such applications because the center of a quadrant detector does not change with time or temperature. The high resolution and accuracy of the quadrant detector senses even small drifts of the beam away from center. Nulling is controlled by a computer that processes the signals from the detector and adjusts a pointing mirror to re-center the beam. Because CVI Melles Griot quadrant detector systems provide beam position information in real time, such alignment can be maintained with high precision and stability.

Other Measurements

PSDs can be used in many more measurement applications, including rotation measurement, linear displacement, and vibration analysis, as shown in figure 11.18.

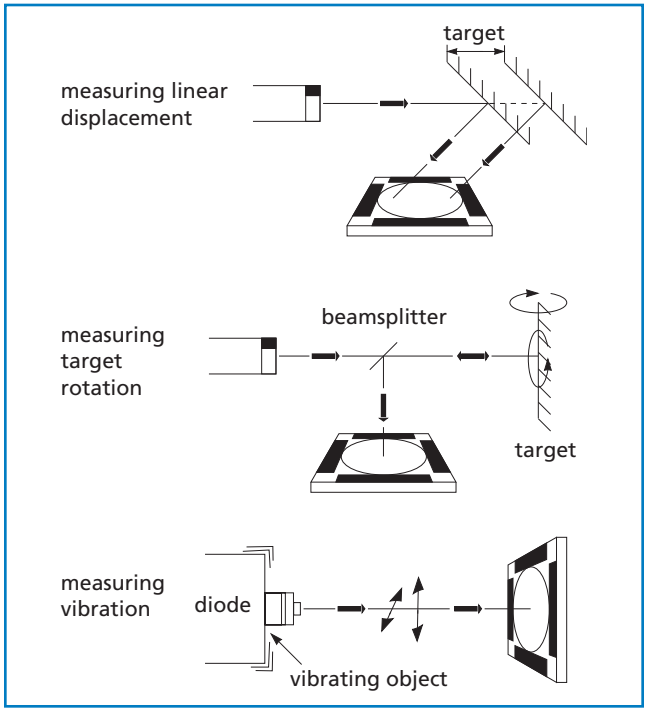

Figure 11.18 **Other types of measurements**

Fundamentals of Spectral Analysis

The Fabry-Perot Spectrum Analyzer

A Fabry-Perot interferometer can be used as a filter to produce an extremely narrow linewidth, or it can be used with a detector to resolve fine spectral details. Its passband is typically in the range of 5×10^{-5} to 10^{-1} cm^{-1} (1.5 MHz to 3 GHz). By physically adjusting the cavity spacing, this passband can be made to scan over a small wavelength region to allow precise spectral tuning. An optical spectrum analyzer based on this interferometer can really be thought of as a very-high-resolution spectrometer with a relatively narrow range of spectral coverage.

FABRY-PEROT INTERFEROMETER THEORY

The Fabry-Perot interferometer is a simple device which relies on the interference of multiple reflected beams. Figure 11.19 shows a schematic of a Fabry-Perot cavity.

Incident light undergoes multiple reflections between the coated surfaces which define the cavity. Each transmitted wavefront has undergone an even number of reflections (0, 2, 4, . . .). Whenever there is no phase difference between emerging wavefronts, interference between these wavefronts produces a transmission maximum. This occurs when the optical path difference is an integral number of whole wavelengths, i.e., when

$$m\lambda = 2t_{op}\cos\theta + \delta \qquad (11.16)$$

where

m is an integer, often termed the order
t_{op} is the optical thickness
θ is the angle of incidence, and
δ is the phase change upon reflection (a constant term that can be ignored in most cases).

At other wavelengths, destructive interference of transmitted wavefronts reduces transmitted intensity toward zero (i.e., most, or all, of the light is reflected back toward the source). Transmission peaks can be made very sharp by increasing the reflectivity of the mirror surfaces. A simple Fabry-Perot interferometer transmission curve is shown in figure 11.20. The ratio of successive peak separation to full width at half-maximum (FWHM) transmission peak is termed *finesse*. High reflectance results in high finesse, or high resolution.

Some Fabry-Perot interferometers are constructed from solid materials such as glass or fused silica. For temperature stability reasons, fused silica is preferred. In these interferometers, the gap between the mirror surfaces is fixed for any specific angle of incidence and temperature, and the transmission versus wavelength pattern is stationary. However, in most Fabry-Perot interferometers, air is the medium between high reflectors; therefore, the optical thickness, t_{op}, is essentially equal to d, the physical thickness. The air gap may vary from a fraction of a millimeter to several centimeters. If this gap is made to vary slightly, in a predictable way, the transmission peaks of the Fabry-Perot will shift as a function of wavelength.

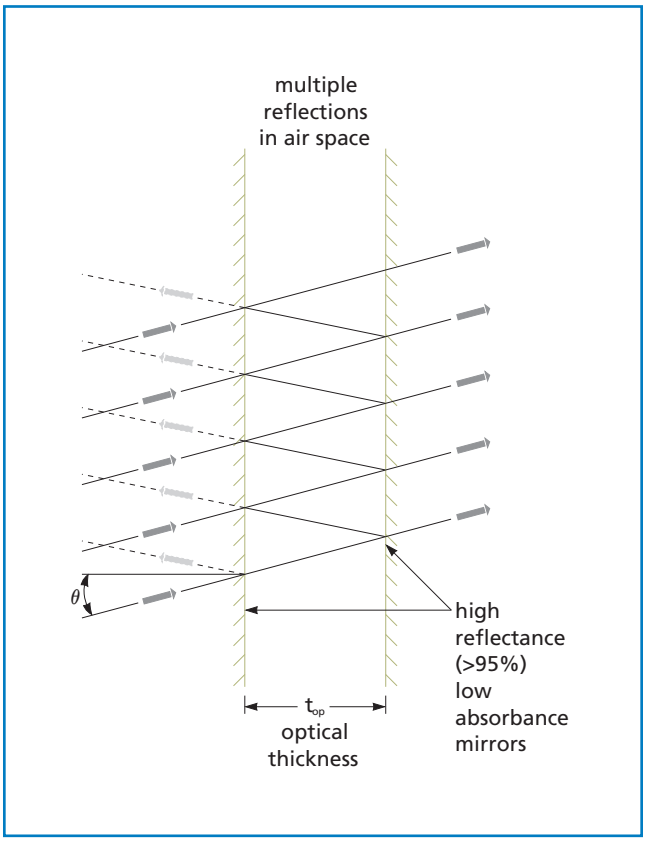

Figure 11.19 **Schematic of a Fabry-Perot Interferometer**

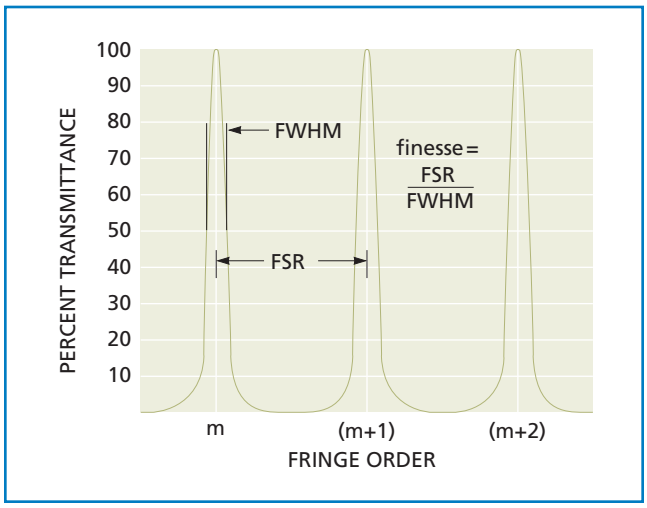

Figure 11.20 **Transmission pattern showing the free spectral range (FSR) of a simple Fabry-Perot interferometer**

As the separation of the mirrors is varied, typically by a ramp voltage applied to piezoelectric spacers, the transmission peak will shift over the FSR (i.e., the frequency space between the adjacent transmission peaks). Each peak occurs when the multireflected beams within the interferometer cavity are in phase at the exit surface. The small percentages transmitted at each reflection (less than one percent) reinforce and produce bright transmission peaks which may then be detected by a silicon or germanium detector.

The art of the Fabry-Perot interferometer design hinges on this apparently simple requirement — controlling the spacing between the mirrors. Even the most minute thermal or mechanical inconsistency will cause the parallelism between the mirrors to change, thus destroying the interference pattern. Great care must be taken in design and manufacture to avoid and prevent these problems and to provide an instrumental solution that is both stable and reliable.

CONFOCAL AND PLANO CONFIGURATIONS

Two practical configurations exist for a Fabry-Perot interferometer: the plano configuration, consisting of a pair of plane-parallel mirrors facing each other, and the confocal configuration, in which the radii of a pair of concave mirrors are equal to their separation. A more general case, in which the radii are substantially longer than the separation, is also possible, but this arrangement can produce anomalous transmission peaks which are difficult to interpret.

For both the confocal and the plano configurations, each spectral component of the incoming radiation produces a transmission peak when the cavity mirror separation d matches a multiple of the spectral wavelength λ. The relationship for a confocal configuration is $d=m\lambda/4$, where m is a large integer called the fringe order. In this instance, the optical round-trip path is four passes through the cavity. For the plano configuration, a round trip consists of only two passes, and the relationship is $d=m\lambda/2$ (ignoring phase changes on reflection). Thus, for any wavelength there will be a transmission peak every time the scanning mirror separation gives an integral value of m for that wavelength.

This results in a spaced-apart, comblike structure of transmission peaks corresponding to the different integral values of m. For each and every spectral line or mode in the incoming beam there will be a similar comb of peaks, and thus a sequence of identical spectra will be displayed across the screen as the mirror separation is ramped through a succession of interference orders m. Adjacent fringe orders are separated by the FSR — $c/4d$ Hz for the confocal configuration and $c/2d$ Hz for the plano configuration. In both cases, the separation between peaks is linear with frequency, as shown in the real-world example given in figure 11.21.

Note, however, that if the range of incoming wavelengths is greater than the FSR of the interferometer, there will be an overlapping of different fringe orders, and the displayed spectrum will be confusing and difficult to interpret.

The sharpness of individual peaks (the resolution of the spectral analyzer) is a function of the "finesse" of the Fabry-Perot interferometer. The value of the overall finesse is determined by the reflectance of the mirrors (the reflectance finesse, $\mathcal{F}_r$, given by:

$$\mathcal{F}_r = \frac{\pi\left(R_1R_2\right)^{1/4}}{1-\left(R_1R_2\right)^{1/2}} \qquad (11.17)$$

where R_1 and R_2 are the reflectances of the two mirror coatings) and the quality of the interferometer's construction (the defect finesse, $\mathcal{F}_d$). As the finesse increases, the peaks of the transmission spectrum become narrower. Normally, reflectance finess predominates unless cavity spacing is very small. Overall transmission, however, may drop as the result of increased absorption. When the reflectance of both interferometer mirrors is the same (i.e., $R_1=R_2=R$), as is the case with a spectrum analyzer, the formula for reflectance finess becomes

$$\mathcal{F}_r = \frac{\pi\left(R\right)^{1/2}}{1-R}. \qquad (11.18)$$

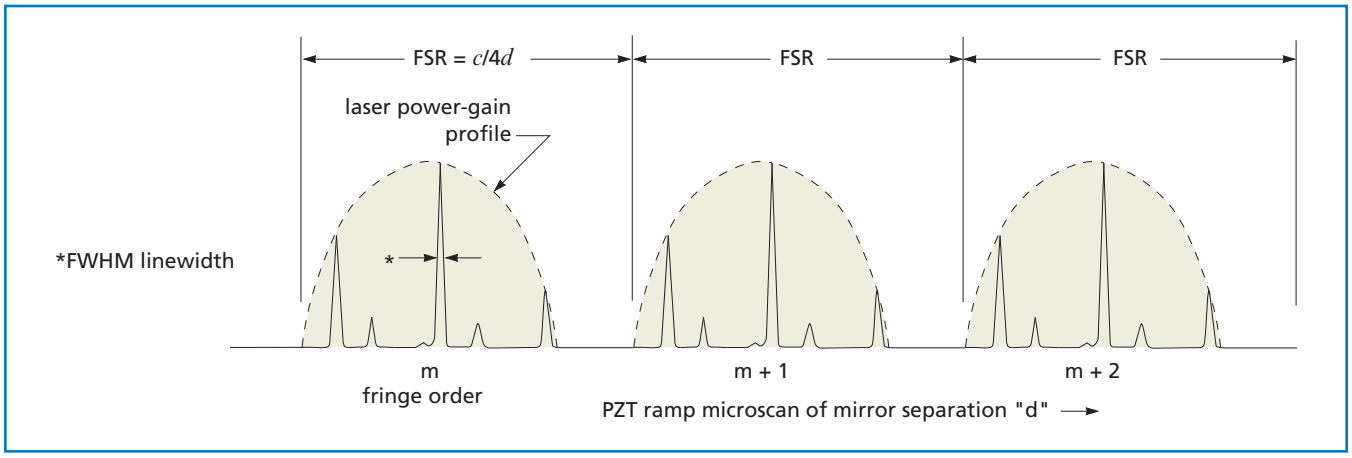

Figure 11.21 **A confocal interferometer scan over three free spectral ranges showing the output of a helium neon laser.**

The FWHM is given by the ratio of the FSR to the finesse. Thus, for a high-resolution spectrum, the FSR should be small and the finesse high.

The defect finesse results from the inevitable residual imperfections in manufacture. As the cavity spacing becomes small, overall surface defects, such as deviation from absolute parallelism or from absolute flatness (sphericity in a confocal interferometer), tend to predominate, but surface microroughness also contributes to the total defect finesse value.

SPECTRUM ANALYZER CONFIGURATION

Laser spectrum analyzers are most often based on the confocal Fabry-Perot design. The common focus and the reentrant optical path leads to very low diffraction losses, good light-gathering capacity (*étendue*) , and easy alignment of the cavity to the laser's optical beam. A major advantage of the confocal design is that the cavity modes are degenerate in frequency. No mode-matching is needed, and each observed laser line or mode represents a genuine signal, not just an instrumental artifact, as can so easily happen with other curved mirror arrangements. Indeed, the confocal spectrum analyzer shown in figure 11.22 should normally be operated slightly misaligned to the laser beam so that there is less chance of feedback to the laser source and resultant mode pulling. This misalignment is achieved without the excitation of spurious interferometer modes. Nonconfocal interferometer arrangements suffer primarily from their need to be mode-matched to the incoming laser beam. Failure to do this will cause spurious transmission fringes resulting from the higher-order transverse modes in the interferometer itself. Unfortunately, it is very difficult to separate stray data generated from these fringes from actual data from the laser beam under test. Other problems, such as the need to optically isolate the interferometric cavity from the laser cavity and the requirement that the laser operate in only a single transverse mode, compound the difficulty of using a nonconfocal Fabry-Perot for spectral analysis. The confocal spectrum analyzer avoids these problems; it is simple to align and adjust, and its output is easy to interpret.

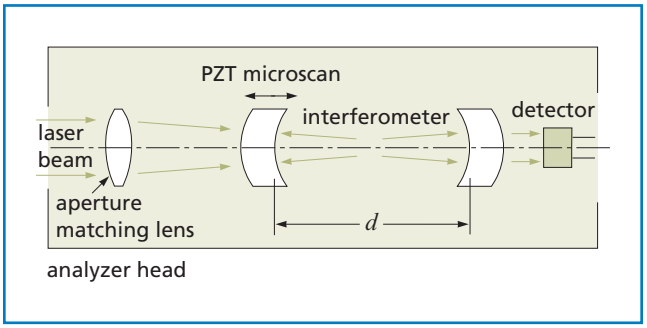

Figure 11.22 **A schematic diagram of a spectrum analyzer**

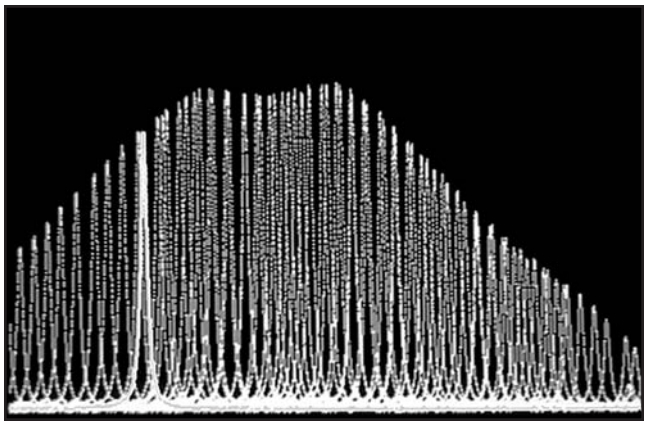

Figure 11.23 **Lasing medium gain curve traced by oscilloscope with spectrum analyzer**

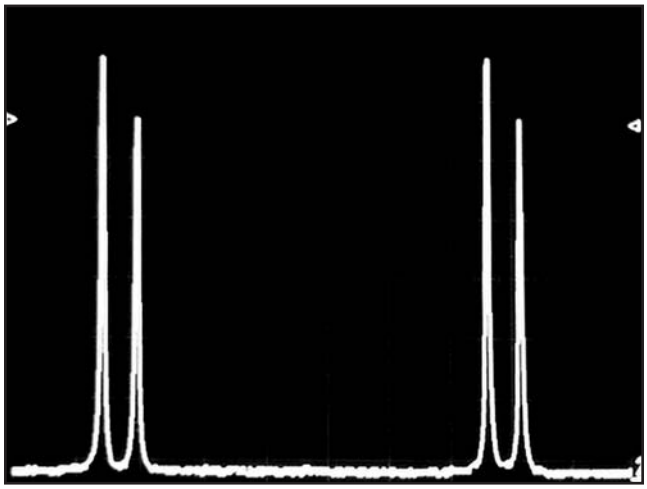

Figure 11.24 **Two laser modes displayed twice during spectrum analyzer scan**

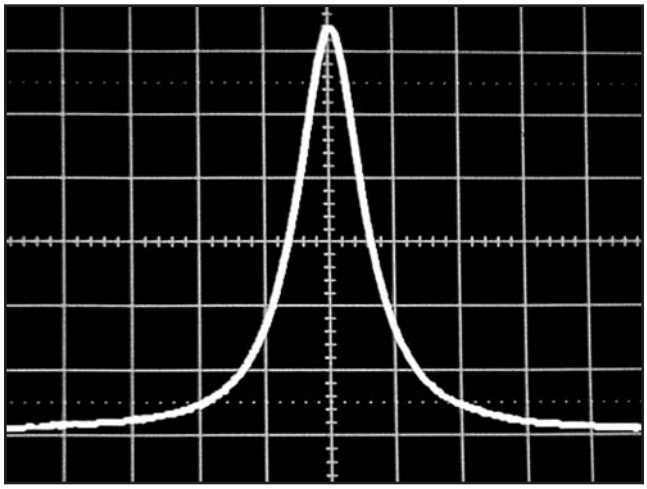

Figure 11.25 **Single mode display using spectrum analyzer**

Measuring Wavelength

When working with a laser, it is usually quite important to know the wavelength the laser is producing. With many this is not typically a problem because the wavelength is defined to within a small fraction of a nanometer by the physics of the lasing system. The red helium neon line is always at 632.8 nm, the main blue argon-ion wavelength is always at 488.0 nm, and so forth. However, when working with a tunable wavelength laser, or a laser than can experience significant wavelength drift as a function of temperature (e.g., a typical semiconductor diode laser), having an instrument available to determine the wavelength quickly with an acceptable level of accuracy is very useful.

Many systems have been developed over the years to measure the wavelength of light, whether from a laser, a lamp, or the output of an optical experiment. Traditionally, the light to be measured was collected and fed into a spectrometer or grating monochromator. If the native accuracy of the monochromator readout was not sufficient, the result could be compared to the readout for closely spaced atomic lines from a spectral source that bracketed the unknown wavelength, using proportional techniques. For highly accurate readings, however cumbersome long-path instruments were required, and, under the best of circumstances, wavelength measurement was a time-consuming task.

The advent of computers gave rise to a new class of instruments, the wavemeter, a table-top instrument that one could shine the unknown light into and receive an immediate readout of the wavelength to a level of accuracy that rivaled the best monochromator systems.

INTERFEROMETRIC WAVEMETERS

For absolute accuracy and precision wavemeters, interferometric techniques have proven the most practical. One common device is based on the scanning Michelson interferometer shown in figure 11.26.

The incident beam is split between a fixed path and a smoothly varying path. Both beams are reflected back and recombined at the beamsplitter to produce a sinusoidal interference pattern which results from the smoothly changing phase relationship between the beams. The unknown wavelength of the incident light, λ, can be calculated using the Michelson interferometer equation:

$$m\lambda = 2nd. \qquad (11.19)$$

In this equation, m is the number of fringes recorded as the scanning mirror of the Michelson interferometer moves through the distance, d. The refractive index, n, of the medium (typically air) between the mirrors of the interferometer is included to account for the difference between the physical path distance and the optical path distance. The accuracy of this wavelength calculation depends primarily on the precision to which the

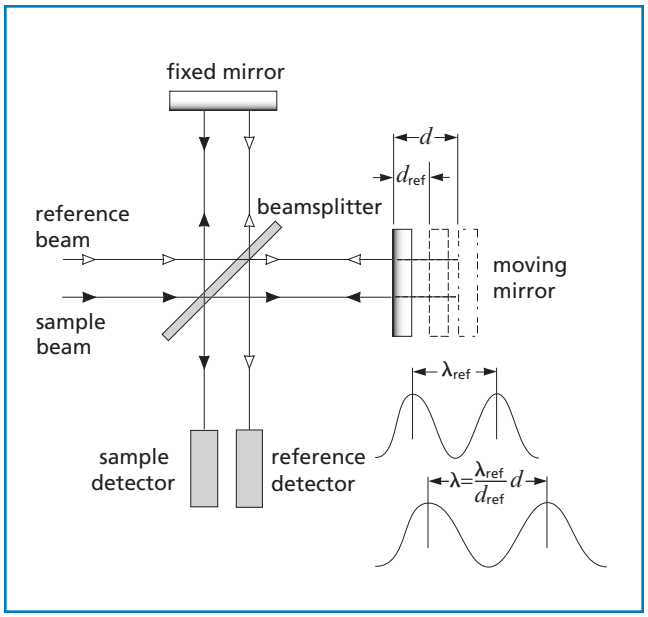

Figure 11.26 **A Michelson interferometer-based wavemeter**

displacement of the scanning mirror is known. In order to obtain highly accurate wavelength measurements, a reference laser with an accurately known wavelength is measured simultaneously to determine the scanning mirror displacement in terms of this wavelength. With this type of instrument, measurements with an accuracy of ± 2 ppm can be obtained.

Interferometric wavemeters can be very accurate, but they are also very expensive, making them unsuitable for routine laboratory applications requiring accuracy of a few tenths of a nanometer.

SEMICONDUCTOR-BASED WAVEMETERS

A new technique, used in the WaveMate™, may be the optimum solution for every-day low-resolution (~0.5 nm) measurements. In this technique, wavelength measurement is accomplished with a single photosensor consisting of two stacked silicon photodiodes, as shown in figure 11.27.

The absorption characteristics of the first photodiode acts as a filter for the second photodiode. The two photodiodes have different spectral response curves (see figure 11.29).

By comparing the output of the two photodiodes, an intensity-independent signal unique for the wavelength of the incident beam is obtained.

WaveMate consists of a sensor head and a console for processing and display. The sensor head contains the photodiode, photoamplifiers, thermostat and a variable neutral density filter. In the console both signals are error corrected and the wavelength is then calculated and displayed.

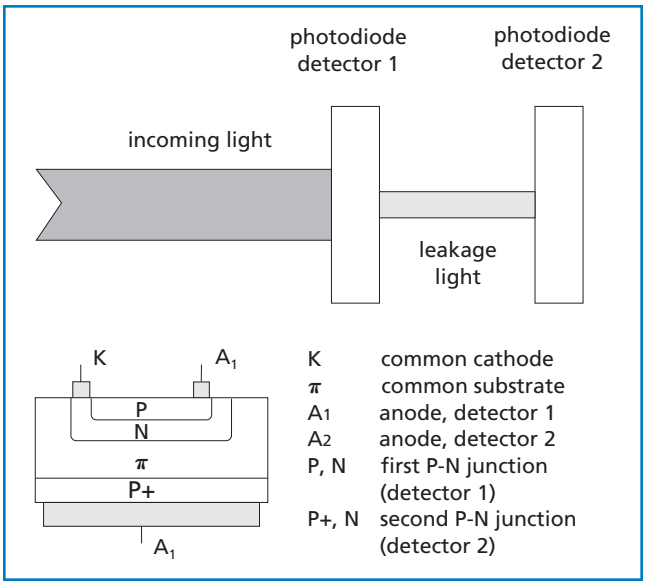

Figure 11.27 **Dual-photodiode wavelength sensor structure**

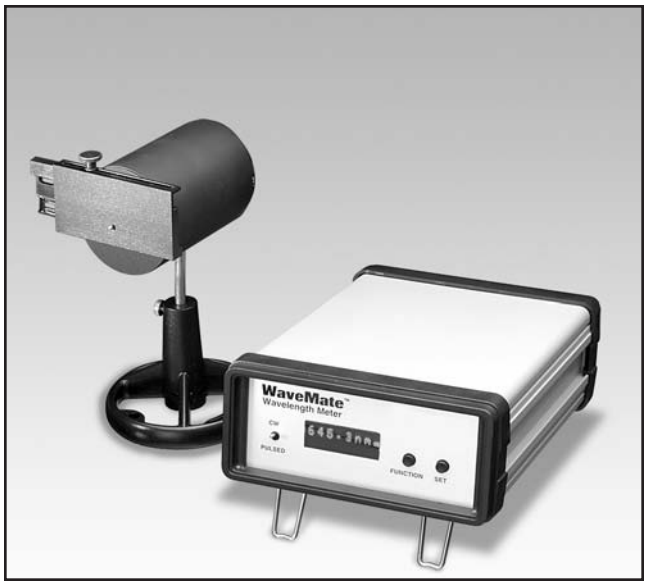

Figure 11.28 **WaveMate™ wavelength meter**

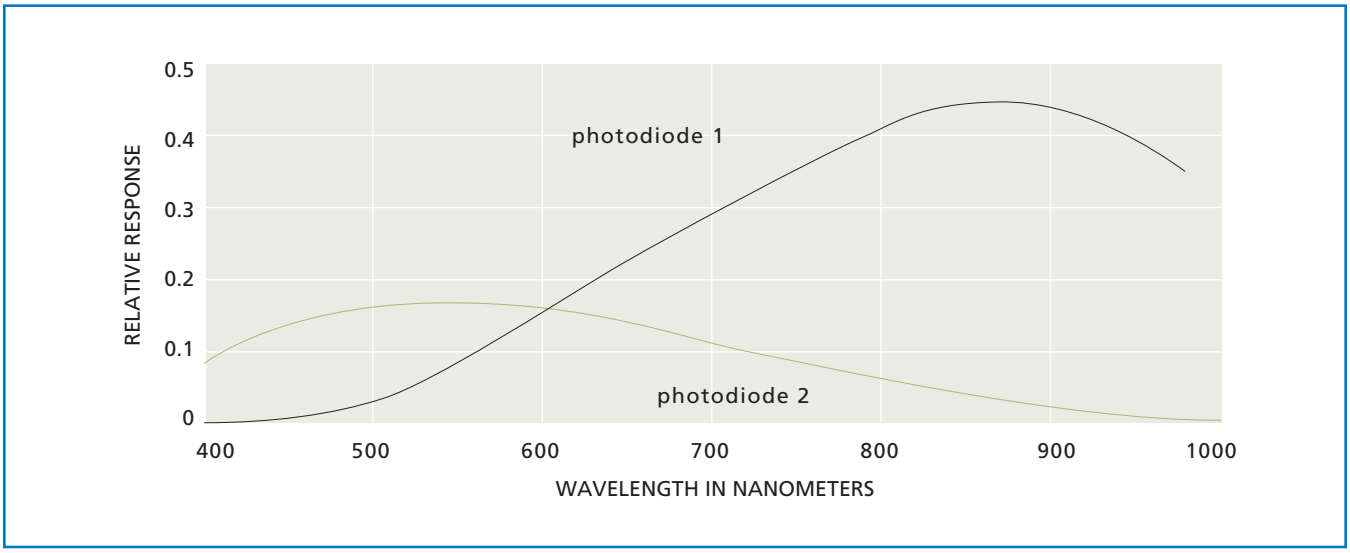

Figure 11.29 **Spectral response curves of the photodiodes**

Spectrometers, Monochromators, and Spectrophotometers

A spectrometer is an instrument used to determine the wavelengths (and their relative intensities) present in a source of light. A monochromator is an instrument used to separate out a single specific wavelength or wavelength band present in a source of light. The spectrophotometer is an instrument used to determine the wavelengths present in the light reflected from an object.

All of these instruments share the same basic operating principal—light from a source passes through, or is reflected by, a dispersing element which spreads the light into its spectral colors. A detector then measures the intensity of the output at various points in the spectrum. The distinction among the instruments, illustrated in figure 11.30, is in the configuration of the source of light, the dispersing element, and the detector.

In a spectrometer, the source is a lamp (or the output of an experiment), the dispersing element is stationary, and the detector is an array of detectors.

In a monochromator, the source is a lamp (or the output of an experiment), the dispersing element rotates, and a single detector is fixed in place.

In a spectrophotometer, the source is the light reflected from a sample, the dispersing element is stationary, and the detector is an array of detectors.

In most cases, the dispersing element is a ruled or holographic grating. In the monochromator, the detector is typically a photodiode or a photomultiplier tube. In the spectrometer and spectrophotometer, the detector is typically a linear CCD or CMOS detector with individual pixel readouts.

SPECTROMETER THEORY

A Czerny-Turner spectrometer is shown schematically in figure 11.31.

Light enters the optical bench through a slit and is collimated by a spherical mirror. A plane grating diffracts the collimated light; a cylindrical mirror then focuses the resulting diffracted light. An image of the spectrum is projected onto a one-dimensional linear detector array.

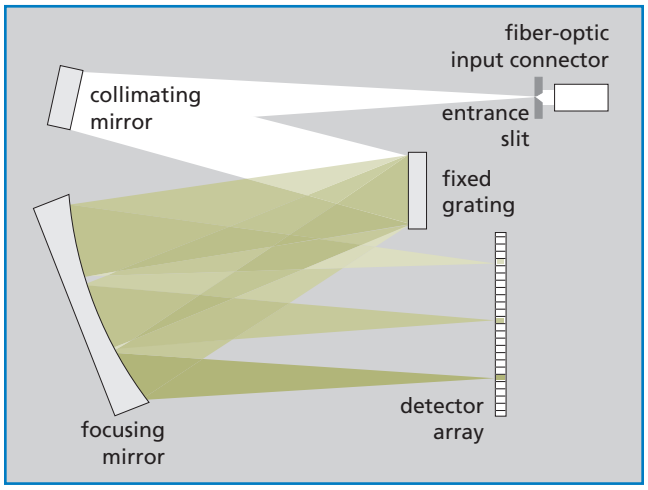

Figure 11.31 **Schematic of symmetric Czerny-Turner spectrometer**

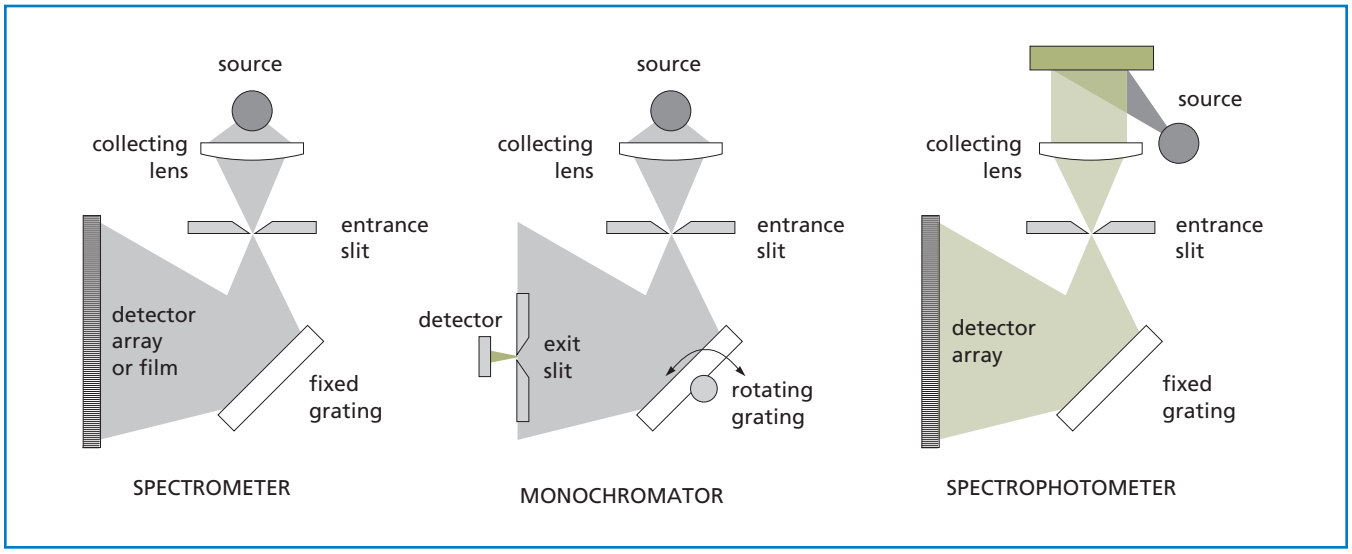

Figure 11.30 **The spectrometer family**

The fundamental grating equation is as follows:

$$\sin\alpha + \sin\beta = 10^{-6} kn\lambda \qquad (11.20)$$

where

α is the angle of incidence in degrees
β is the angle of diffraction in degrees
k is the diffraction order (an integer)
n is the grating density in lines/mm
λ is the wavelength of light in nm

and the angular separation (angular dispersion) between two wavelengths, in radians, is given by

$$\frac{d\beta}{d\lambda} = \frac{kn}{\cos\beta} \times 10^{-6} \qquad (11.21)$$

The separation of the wavelengths at a detector is defined as the linear dispersion of the system. For a detector that is perpendicular to the diffracted beam (the case for a monochromator), linear dispersion is given by

$$\frac{d\lambda}{dx} = \frac{\cos\beta}{knL_b} \times 10^{-6} \qquad (11.22)$$

where L_b is the distance from the focusing lens to the detector. For a spectrometer with a planar detector (see figure 11.32) , the distance L_b changes with β, and the linear dispersion formula becomes

$$\frac{d\lambda}{dx} = \frac{\cos\beta\cos^2\gamma}{knL_h} \times 10^{-6} \qquad (11.23)$$

where

$\gamma = \beta_h - \beta$
β_h=is the angle between the perpendicular to the detector and the grating normal
L_h=the perpendicular distance from the focusing lens to the detector.

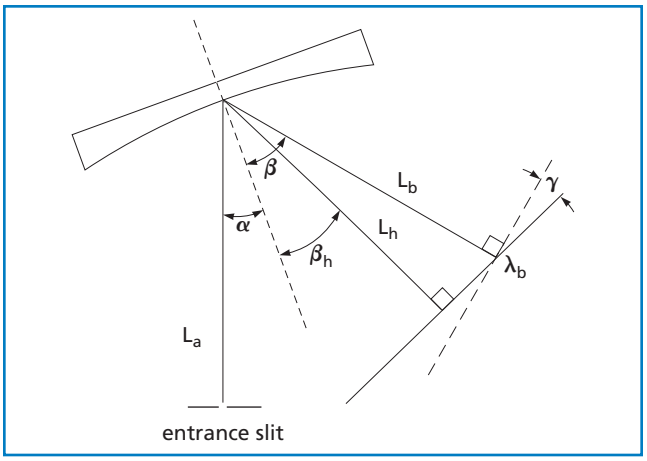

Figure 11.32 **Spectrometer configuration** (curved grating replaces planar grating and focusing lens.)

From these equations it is clear that increasing the distance from the focusing mirror to the detector spreads the spectrum over a wider area, increasing the dispersion and, in principle, increasing the resolving power of the instrument.

RESOLVING POWER

Resolution is the ability of an instrument to separate adjacent spectral lines, and is given by the equation

$$R = \frac{\lambda}{\delta\lambda} \qquad (11.24)$$

where $\delta\lambda$ is the difference in wavelength between two spectral lines of equal intensity. It may be shown that

$$R = \frac{\lambda}{\delta\lambda} = knW_g = kN \qquad (11.25)$$

where

W_g=the illuminated width of the grating and
N=the total number of grooves in the gratings.

Using the earlier equations, it can also be shown that

$$\frac{d\lambda}{dx} = Wg\frac{\sin\alpha + \sin\beta}{\lambda} \times 10^{-6} \qquad (11.26)$$

Obviously, the resolving power of a spectrometer depends on the width of the grating, the geometry, and the wavelength to be resolved. The size of the incoming light at the entrance aperture is determined by the slit width or, in the absence of a slit, the fiber diameter.

WAVELENGTH AND ORDER

Unlike a dispersing prism, a diffraction grating does not produce a single spectra, but instead it produces multiple spectra determined by the equation

$$k\lambda = \text{constant} \qquad (11.27)$$

where k is an integer. Consequently, for a broad spectral source, the spectra will overlap. For example, at the detector location for 800 nm, output at 400 nm, 266.6 nm, and 200 nm will also be present. Consequently, filters must be used to eliminate the higher-order spectra.

BLAZED GRATINGS

Blazed gratings are designed to produce maximum efficiency at a specific wavelength. This is accomplished by forming the grooves in such a manner that the incident and refracted angle, at that wavelength, are equal (the Littrow condition). A grating that is blazed for a first-order wavelength, will also be blazed for the corresponding higher-order wavelengths.

Fundamentals of Beam Profiling and Beam Measurement

As a laser beam propagates, its width and spatial intensity distribution will change in space and time owing changes in the laser cavity, divergence, and interaction with optical elements. Spatial intensity distribution is one of the fundamental parameters that indicates how a laser beam will behave in an application. Laser printing, material processing, fiber optic coupling, optical data storage, laser pumping, and photochemistry are some of the applications whose efficiency depends on a laser's spatial intensity profile and beam width. Theory can sometimes predict the behavior of a beam, but manufacturing tolerances in lenses and mirrors, and ambient conditions affecting the laser cavity, necessitate verification. Consequently, it is crucial for researchers, system designers, and laser manufacturers to be able to measure accurately these parameters. ISO standard 11146 defines approaches to be used in measuring such beams. All CVI Melles Griot products are in full conformance with this standard.

DEFINING BEAM WIDTH

The boundaries of optical beams are not clearly defined and, in theory at least, extend to infinity. Consequently, the dimensions of a beam cannot be defined as easily as the dimensions of hard physical objects. The commonly used definition of beam width is the width at which the beam intensity has fallen to $1/e^2$ (13.5%) of its peak value when measured in a plane that is orthogonal to the optical axis. This is derived from the propagation of a Gaussian beam and is appropriate for lasers operating in the fundamental TEM_{00} mode (see figure 11.33).

Many lasers, however, exhibit a significant amount of beam structure, and applying this simple definition leads to problems. Therefore, the ISO 11146 standard specifies the beam width as the $1/e^2$ point of the second moment of intensity, a value that is calculated from the raw intensity data and which reduces to the common definition for a Gaussian beam.

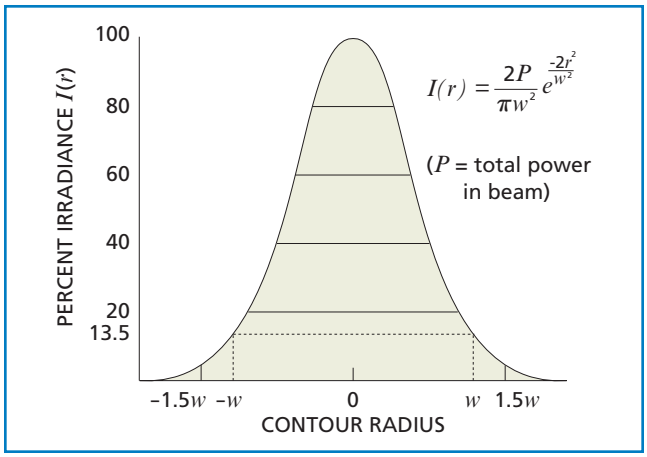

Figure 11.33 **Gaussian profile of a TEM_{00} mode** (note the beam radius w at the $1/e^2$ (13.5%) intensity level)

METHODS OF MEASURING BEAM WIDTH

There are four main types of beam-profiling instrumentation: camera-based systems, knife-edge scanners, slit scanners, and pinhole scanners. Each has specific advantages and disadvantages. Different measurement techniques may result in slightly different results; therefore, it is critical that comparative measurements be made with the same technique.

Camera-Based Profilers

Camera-based profilers use a two-dimensional array of square or rectangular pixels as the imaging device,which, much like photographic film, instantly record and display the entire optical pattern that impinges on the camera surface. The intensity distribution of a laser beam is recorded pixel by pixel and displayed as either a topographic or three-dimensional contour plot. The advantage of such profilers is that they can detect and display any structure that may exist on the profile. They can display two- and three-dimensional plots of profiles, and they can be used with both cw and pulsed lasers. The chief disadvantage of these instruments is that their measurement resolution is limited by pixel size (usually between 5 and 10 μm on a side), which, in general, limits their use to measuring beams greater than ~60 μm in width. A new class of camera-based profiler, the μBeam™, overcomes this size limitation by magnifying the laser beam, in a calibrated manner, by a factor of up to 100 × . This allows profiling of beams less than 5 μm in diameter but limits the maximum beam diameter to about 50 μm. Another disadvantage is limited spectral range.

Two types of image detectors are used in CVI Melles Griot beam camera-based profilers—charge-coupled device (CCD) detectors and complementary metal-oxide semiconductor (CMOS) detectors. In general, CCD detectors have a greater dynamic range and lower noise than CMOS detectors, but they are somewhat slower and require much more complex circuitry. In camera-based beam profilers, the performance differences are minor. One clear advantage of a CMOS detector is that the failure of pixel can shut down a complete row because of the way in which charge travels through the detector.

Knife-Edge, Slit, and Pinhole Profilers

All three of these instruments generate a profile by mechanically moving an aperture across the beam in a plane orthogonal to the optical axis. The light passing through the aperture is measured by a detector and correlated with the position of the aperture as it crosses the beam. Unlike camera-based scanners, which measure a profile in three dimensions (x, y, intensity), scanners measure only two dimensions at a time (x and intensity or y and intensity). Consequently, three-dimensional representations generated by these systems are calculated, not measured, and the accuracy or the reconstruction depends upon basic assumptions made about the beam characteristics and the algorithms used in the reconstruction.

Scanning Pinhole Profilers

Pinhole profilers use a small pinhole as the aperture and plot the transmitted power vs position. The resolution of the profile is determined by the size of the aperture. The chief advantage of a pinhole profiler is its ability, within the resolution, to create an exact profile of a plane through a portion of the beam. The disadvantages are that the transmitted power through the pinhole is very small, aligning the pinhole is extremely difficult, and multiple positional measurements are needed to generate a profile of the entire beam.

Scanning Slit Profilers

Slit profilers use a long narrow aperture which encompases the full width of the beam in a direction perpendicular to the travel of the slit. It then plots the transmitted power through the slit vs position. Unlike the pinhole scanner, the slit scanner scans through the entire beam, not just a single plane. However, unless the beam is circularly symmetric and near Gaussian, the profile may not be an exact representation of the intensity profile. Like pinhole scanners, the resolution of the scan is a function of the width of the slit, and the narrower the slit, the less light reaches the detector, decreasing the signal-to-noise ratio.

Scanning Knife-Edge Profilers

Knife-edge profilers use an aperture large enough to pass the entire beam. The aperture has one sharp, straight edge (knife edge). As the aperture traverses the beam, the system measures the portion of the beam that is not blocked by the blade (see figure 43.34) and plots the differential (rate of change in intensity) vs positon of the power through the aperture.

This has several advantages when compared to a slit or pinhole scans: The beam intensity is not limited by the size of the pinhole or slit width, so the signal-to-noise ratio is very high; resolution is not limited by the size of the aperture, allowing beams of a few microns in diameter to be measured; and because, at some point in the scan the full beam strikes the detector, accurate power and noise measurements can be taken. Like the slit scanner, the accuracy of a scan depends upon the geometry of the beam. For best results, the beam should be circularly symmetric and near Gaussian.

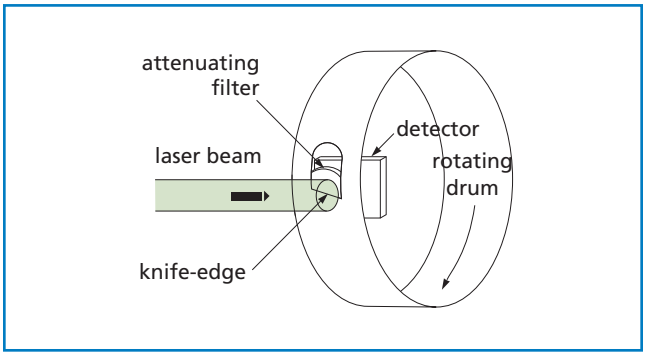

Figure 11.34 **Simplified mechanics of a knife-edge beam profiler**

Tomographic Scanning

As discussed above, scanning slit and knife-edge scanners cannot generate truly accurate three-dimensional reconstructions of laser beam profiles. Reasonable approximations can be made, however, by using tomographic techniques—the same techniques used with MRI and CAT scanners to create three-dimensional images of internal organs. The key to making these reconstructions is to scan the beam in as many different directions as possible. For useful tomographic analysis, scans from at least three different directions are needed. If scans could be made from 10 or more directions, the three-dimensional reconstruction would be highly accurate.

CVI Melles Griot offers two knife-edge systems that use tomographic algorithms to construct three-dimensional profiles. The BeamAlyzer™ system has a three-blade scan, and the Super BeamAlyzer™ has a seven-blade scan (see figure 11.35). For most beams, the Super BeamAlyzer's reconstructions rival those measured directly with a camera-based scanner.

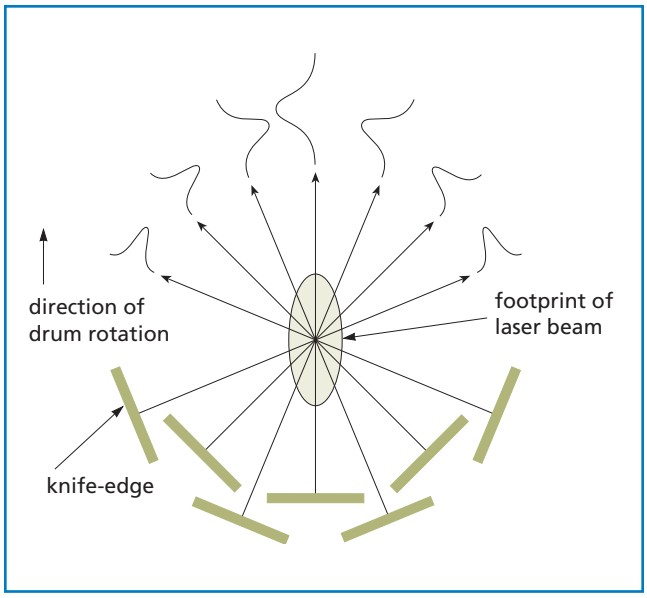

Figure 11.35 **Orientation of the knife edges on the 7-blade Super BeamAlyzer™ tomographic beam profiler**

BEAM PROPAGATION FACTOR AND M^2

The propagation factor k is given by the equation

$$k = \frac{1}{M^2} = \frac{\lambda}{\pi W_0 \theta} \qquad (11.28)$$

where λ is the wavelength of the beam, W_0 is the beam waist, and θ_0 is the far-field divergence of the beam. The propagation factor is an invariant that describes the relationship of a non-Gaussian beam to a Gaussian beam as it passes through an optical system. If $k=M=1$, the beam is Gaussian. If k<1 ($M^2>1$), the beam is not Gaussian, but all of the standard Gaussian propagating formulas may be used with appropriate modifications (e.g., $W_0=M \times w_0$, $\theta_0=M \times \theta_0$ where w_0 and θ_0 are the corresponding Gaussian parameters). Indeed, the concept of an "embedded Gaussian" has been introduced as a construct to assist with both theoretical modeling and laboratory measurements (see figure 11.36).

M^2 Measurement

A variety of instruments have been developed to measure the propagation factor and M^2 in the laboratory. Most are based on the same fundamental operating principle; the incoming laser beam is focused by a lens. This creates a beam that has a beam waist at the focal point, a near-field divergence region (within the Raleigh range), and a far-field region (many, many times the Rayleigh range) all within a distance of a few inches. Using a beam profiler, the beam diameter at the waist and the diameters at near-field and far-field points on either side of the waist are measured. A computer then fits a hyperbolic curve to the data and, using the fundamental Gaussian formulas, calculates the beam waist and divergence of the embedded Gaussian, M^2, the location of the beam waist in the incoming laser beam, and other critical parameters. A schematic diagram of a simple M^2 moving lens device is shown in figure 11.37.

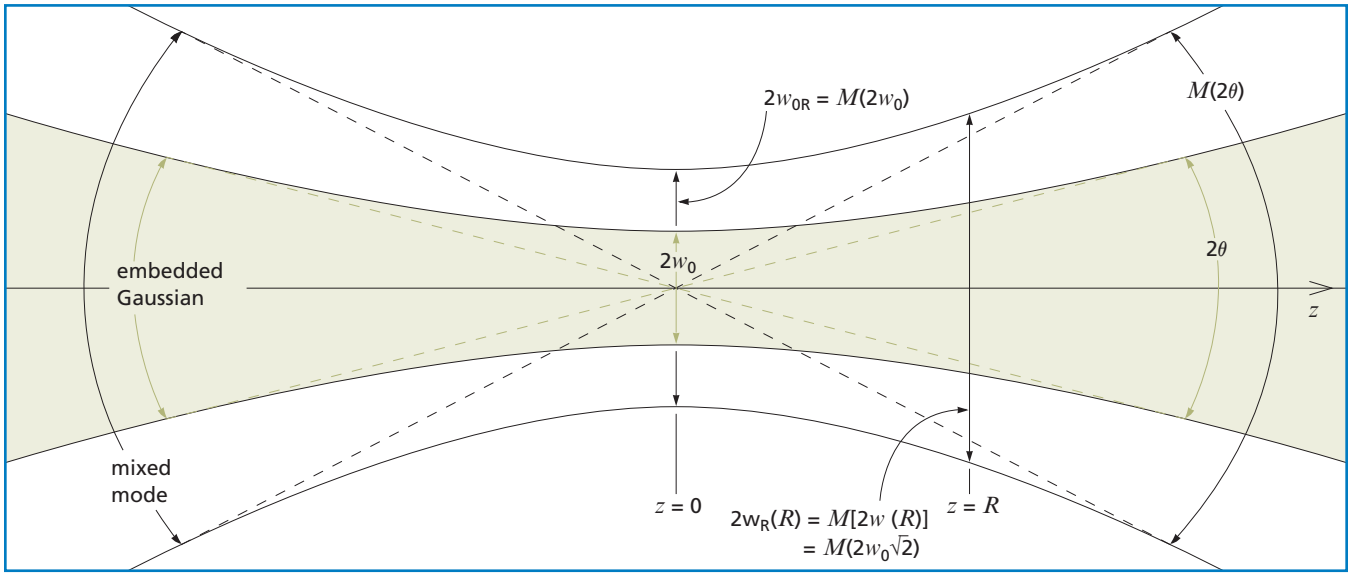

Figure 11.36 **The embedded Gaussian concept** A mixed-mode beam which has a waist M (not M^2) times larger than the embedded Gaussian will propagate with a divergence M times greater than the embedded Gaussian, and the mixed-mode width will always be M times the embedded Gaussian width, but will have the same radius of curvature and the same Rayleigh range

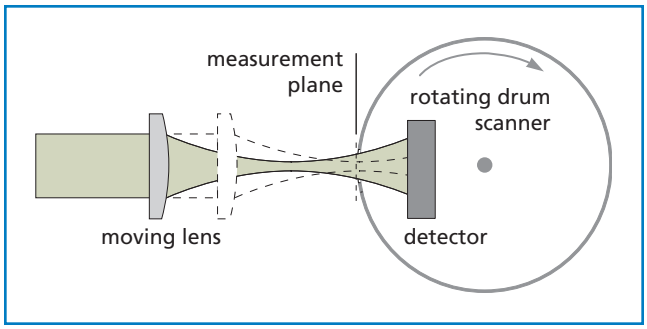

Figure 11.37 **A simple moving-lens M^2 setup**